Study on the Molecular Basis of Huanglian Jiedu Decoction Against Atopic Dermatitis Integrating Chemistry, Biochemistry, and Metabolomics Strategies

Jing Chen[1†], Saizhen Chen[2†], Jinguang Chen[3], Bixin Shen[4], Zhengli Jiang[1] and Yubin Xu[2]*

[1]Department of Pharmacy, Taizhou Hospital of Zhejiang Province Affiliated to Wenzhou Medical University, Lin Hai, China, [2]Department of Pharmacy, Taizhou Central Hospital (Taizhou University Hospital), Taizhou, China, [3]Department of Dermatology, Taizhou Central Hospital (Taizhou University Hospital), Taizhou, China, [4]Department of Pharmaceutics, School of Pharmaceutical Sciences, Wenzhou Medical University, Wenzhou, China

Atopic dermatitis (AD) is a common chronic relapsing skin inflammation, which severely affect the quality of life of patients. Inhibiting itching and enhancing immunity to mitigate scratching are key elements in the fight against AD. Huanglian Jiedu decoction (HLJDD) has multiple pharmacological effects in the treatment of AD. However, the effective ingredients and underlying molecular mechanisms have not yet been fully explored. Thus, this study integrates chemistry, biochemistry, and metabolomics strategies to evaluate the active substance basis of HLJDD against AD. First, HLJDD was split to five fractions (CPF, 40AEF, 90AEF, PEF and WEF) and 72 chemical components were identified. NSD (Non-similarity degree) among the different fractions showed significant chemical differences (>81%). Interleukin IL-13, IL-17A, IL-3, IL-31, IL-33, IL4, IL-5, TSLP, IgE, and histamine in the serum, and IL-4Rα, JAK1, and HRH4 levels in skin, participating in inhibiting itching and regulating immunity signaling, were found to be restored to varying degrees in AD treating with HLJDD and its fractions, especially 40AEF and CPF. Untargeted metabolomics analysis demonstrated that forty metabolites were differential metabolites in plasma between the HLJDD-treated group and the AD group, involving in histidine metabolism, arginine biosynthesis, pyrimidine metabolism, and so on. Further, targeted metabolomics analysis revealed that eleven differential metabolites, associating with physiological and biochemical indices, were significant improved in the HLJDD and its fractions groups. In conclusion, HLJDD exhibited anti-AD effects by inhibiting itching and enhancing immunity, which in turn regulating the levels of relative metabolites, and CPF and 40AEF were considered the most important components of HLJDD.

Keywords: huanglian jiedu decoction, atopic dermatitis (AD), metabolomics, molecular basis, mechanism

INTRODUCTION

Atopic dermatitis (AD), also known as atopic eczema, is a common chronic relapsing skin inflammation (Serrano et al., 2019). AD has a high incidence in developed countries, with a prevalence of up to 10–20% in Korea, Japan, Europe, and United States (Kim et al., 2016). As a result of rapid urbanization, the prevalence of AD has increased worldwide (Daya and Barnes, 2019). In China, a higher regional prevalence has been observed in coastal cities. Although AD is not uniformly lethal, it has a long disease duration and persistent symptoms, such as dryness, itching, and roughness, which severely affect the quality of life of patients, exerting a significant economic burden (Eckert et al., 2019; Olsson et al., 2020), especially in individuals with skin infections (Sandhu et al., 2019).

AD pathogenesis is a complex disorder that is considered to arise through a combination of genetic, immunological, environmental, skin barrier, and skin microbiota factors. Among these, skin barrier damage and immunologic dysfunction are considered critical factors (Bonamonte et al., 2019). Recent studies have shown that eosinophils and mast cells are the most important effector cells in AD, releasing inflammatory mediators, such as histamine, leukotrienes, and cytokines (IL-3, IL-4, IL-5, and IL-13), which ultimately leads to itching and skin lesions, which are characteristic of AD (Raap et al., 2006; Lam, 2010). A large number of CD4^{+} T-cell infiltrates were observed in AD. CD4^{+} T cells exhibit a variety of biological functions, including secretion of cytokines for immune regulation and effector function, which are divided into Th1 and Th2 subsets (Sur et al., 2016). Th2 cells secrete cytokines such as IL-4, IL-5, and IL-13, which are important for AD development, especially in the acute phase of AD. IL-4, IL-5, and IL-13 induce B cell activation to produce IgE, and there is a positive correlation between IgE and IL-4 levels. Mast cells were recruited by chemokines and activated by IgE or non-IgE factors. Finally, mast cells produce a range of inflammatory factors, which interact with nerve cells, T cells, eosinophils, and keratinocytes, and participate in the process of skin itch and inflammatory reactions in AD. In addition, IL-31 was not only strongly associated with pruritus in AD but also exhibited synergy with the H4 receptor, thus aggravating pruritus and skin lesions (Otsuka et al., 2011). Previous studies have indicated that IL-4Rα and JAK1 are key indices of inflammatory chronic itching and non-inflammatory chronic itching, respectively, with IL-4 promoting histamine release and worsening pruritus (Oetjen et al., 2017). Ultimately, skin barrier dysfunction and imbalanced immune function jointly contribute to the development of AD. Therefore, inhibiting itching and enhancing immunity to mitigate scratching are key elements in the fight against AD, which would improve the patient's quality of life. A vast variety of treatments, including emollient, anti-inflammatory, and antimicrobial therapies, have been prescribed for AD. However, even though these treatments seem optimal in many patients, their long-term

use carries the risk of severe systemic and cutaneous adverse effects. For these reasons, patients often seek alternative therapies (Blume-Peytavi et al., 2019). Therefore, a cure for AD requires a new treatment strategy to improve the efficacy and reduce the toxicity of short- and long-term therapeutic regimens.

Huanglian Jiedu decoction (HLJDD), a traditional Chinese medicine, is frequently prescribed due to its effectiveness against a variety of serious illnesses, including those of the skin (Chen et al., 2016). The formula is composed of four Chinese medicines: *Coptis chinensis* Franch.(Huanglian), *Scutellaria baicalensis* Georgi (huangqin), *Phellodendron amurense* Rupr.(huangbai), and *Gardenia jasminoides* J. Ellis (zhizi) at a ratio of 3:2:3:3 (Chen, et al., 2017). Modern pharmacological studies have confirmed that HLJDD has antipyretic, anti-inflammatory, antibacterial, antiulcer, and antitumor properties and promotes phagocytic function. With these properties, HLJDD has a curative effect in the treatment of AD (Qi et al., 2019). Clinical and experimental studies have confirmed that HLJDD is an effective drug for treating AD. However, the effective ingredients and underlying molecular mechanisms have not yet been fully explored (Kobayashi et al., 2004).

Traditional Chinese medicine (TCM) has been used to control and cure diseases for thousands of years. Formulas are a fundamental and unique part of TCM. TCM formulae are designed according to dialectical thinking, holistically and synergistically to maximize their therapeutic effectiveness. TCM formulae contains hundreds of chemical components, wherein each component has a different target, exhibiting extraordinary pharmacological activities (Zhang et al., 2017). In recent decades, decoction or ethanol extracts of Chinese drugs or TCM formulas have been split into different fractions to evaluate their main pharmacodynamic components (Pico-Hernández et al., 2020). However, many similar chemical components exist among the splitting fractions, resulting in a dispersion or loss of pharmacological activity. Hence, there is a need to establish a method with which to evaluate the non-similarity degrees of the splitting fractions.

At present, splitting fractions are characterized by HPLC to evaluate the non-similarity degrees among different fractions (Yuansheng et al., 2006). In our previous study, the chemical compositions of *Atractylodes macrocephala* Koidz. were split into five splitting fractions, and non-similarity degrees were evaluated using a variety of analytical methods (Li et al., 2014a). However, the characterization of these chemical constituents is often identified by HPLC techniques combining pure standards (Maimaiti et al., 2020). There are relatively few chemical constituents for characterization by HPLC, which could result in errors or an incomplete evaluation of non-similarity degrees. So far, there have been few reports on the characterization of chemical constituents of fractions of UPLC-Q-TOF/MS/MS, and almost no research on the evaluation of non-similarity degrees among different fractions. In recent years, LC-MS and UPLC-Q-TOF/MS/

MS have been used to analyze and determine the chemical constituents of Chinese drugs, particularly UPLC-Q-TOF/MS/MS technology (Cao et al., 2015; Ma et al., 2016). Currently, UPLC-Q-TOF/MS/MS is widely used for the analysis of the multiple chemical constituents of Chinese drugs, and is highly accurate, highly efficient, and has a wide molecular mass range (Wang et al., 2015; Yang et al., 2015).

In the present study, the chemical constituents of HLJDD were split using various separation methods, analyzed, and identified by UPLC-Q-TOF/MS/MS technology combined with standard substances and literature. Meanwhile, a DNFB-induced AD model was established and used to explore the effects of HLJDD and its fractions. In addition, untargeted metabolomics analyses were performed to screen potential biomarkers of AD, and targeted metabolomic analyses were performed to elucidate and verify the therapeutic effects of HLJDD and its fractions.

MATERIALS AND METHODS

Chemicals and Reagents

Coptis chinensis Franch.(Huanglian), *Scutellaria baicalensis* Georgi (huangqin), *Phellodendron amurense* Rupr.(huangbai), and *Gardenia jasminoides* J. Ellis (zhizi) were purchased from Hangzhou Mintai (Bozhou) Chinese Herbal Medicine Co. Ltd. (Zhejiang, China) and were certified by the standards elaborated in Chinese Pharmacopeia (2020 edition). Portions of the above four herbs were deposited in the Department of Pharmacy of Taizhou Central Hospital (Taizhou University Hospital), Taizhou, Zhejiang for future reference under reference number Xu1-4. 2,4-dinitrofluorobenzene (DNFB) was purchased from Shanghai McLean Biochemical Technology Co., Ltd. (Shanghai, China).

Methanol, acetonitrile, and formic acid (LC-MS grade) were purchased from CNW Technologies (Germany). Ethanol, petroleum ether, and ethyl acetate (analysis grade) were obtained from Tianjin Damao Chemical Reagent Co., Ltd. (China). The standard substances of baicalin, chrysin, ferulic acid, geniposide, obacunone, wogonin, wogonoside, auraptene, protopine, isochlorogenic acid A, chelerythrine, rutecarpine, palmatine, and berberine were purchased from the resource platform of the National Standard Material (China).

Preparation of HLJDD and Splitting of the HLJDD Fractions

HLJDD was composed of *Coptis chinensis* Franch. 900 g, *Scutellaria baicalensis* Georgi 600 g, *Phellodendron amurense* Rupr. 600 g, and *Gardenia jasminoides* J. Ellis 900 g. The above four Chinese medicines were pulverized and decocted twice by refluxing with water (1:12 w/v) for 2 h, then filtered, and the filtrate was combined and concentrated in vacuum to 0.3 g crude drug per 1 ml and then stored in 4°C for the water decoction of HLJDD. According to the polarity differences of the

chemical constituents of HLJDD, the water decoction of HLJDD was split into crude polysaccharide fraction (CPF), petroleum ether fraction (PEF), water eluted fraction (WEF), 40% ethanol eluted fraction (40AEF), and 90% ethanol eluted fraction (90AEF). The specific processes are described in the **Supplementary Material S1**. Meanwhile, the HPLC fingerprints of four small molecular components (PEF, WEF, 40AEF, and 90AEF) were established using a similarity evaluation system for chromatographic fingerprints of TCM (version 2012A). The chromatographic conditions are described in the **Supplementary Material S1**.

UPLC-Q-TOF-MS/MS Analysis of HLJDD and its Fractions

The chemical constituents of HLJDD and its fractions were analyzed and identified by UPLC-Q-TOF/MS/MS technology combined with standard substances and the literature. Details of the chromatography, mass spectrometry conditions, and data processing are described in **Supplementary Material S2**.

Non-Similarity Degree Evaluation of Chemical Fractions

Given that the overlapping property was small between CPF and other fractions, we only evaluated the NSD of four small molecular components (PEF, WEF, 40AEF, and 90AEF). NSD was evaluated and measured by qualitative analysis and quantitative analysis using HPLC data and UPLC-Q-TOF-MS/MS data.

Principal component analysis (PCA) and hierarchical clustering analysis (HCA) were used to evaluate the NSD of the four fractions. Multivariate analysis was performed using a combination of PCA and the SIMCA-P software (version 14.0). HCA was performed using the OmicShare tools in RStudio.

Based on a previous study (Li et al., 2014b), the standard degree was defined as the overlapping property or similarity degree, and NSD was defined as the un-overlapping property or non-similarity degree among the four fractions. The sum of the similarity degree and NSD was equal to 1. Furthermore, NSD was introduced to measure the un-overlapping property of four fractions by peak areas of crude drug, angle cosine analysis, and correlation coefficient analysis. NSD among different fractions was calculated using the cross-analysis method of peak areas of crude drug, angle cosine analysis method (Wang et al., 2002), and correlation coefficient analysis method (Guo et al., 2014). The specific algorithm for the three methods is described in **Supplementary Material S3**.

AD Model Establishment and Treatment

Male C57BL/6 mice (4–6 weeks), weighing 20 ± 2 g, were purchased from Shrek Jinda Laboratory Animals Co., Ltd. (Hunan, China, Laboratory Animal License #SCXK 2016-0010). The animals were kept under SPF laboratory

conditions and provided with a standard laboratory diet and filtered tap water. All animal experimental procedures were approved by the Bioethics Committee of Shanghai Tenth People's Hospital (ID no. SHDSYY-2020-9001). All experimental animals were acclimated for 1 week before the experiment.

In the present study, reference-dose HLJDD in mice was selected as the clinically equivalent dose of HLJDD in humans (according to the body surface area exchange algorithm of human and mice: HLJDD clinical dose: 30 g/day, adult weight 70 kg, the dose of mice was: 30 g/70 kg × 9.1 ≈ 3.9 g/kg). With this as a reference dose, we have previously shown the effects of different dosages of HLJDD (3.2 g/kg, 6.4 g/kg, and 12.8 g/kg) on the AD model. After the dose-effect experiment, 12.8 g/kg was found to be the effective dose (**Supplementary Material S4**). Therefore, the 12.8 g/kg water decoction of HLJDD and the five fractions with the corresponding extracts (CPF: 921.6 mg/kg, 40AEF: 458.24 mg/kg, 90AEF: 460.8 mg/kg, WEF: 1.0086 g/kg, PEF: 1.38 mg/kg) were used to evaluate the mechanism and substance basis of Huanglian Jiedu decoction against AD. Then, C57BL/6 mice were randomly divided into 8 groups (8 mice per group): normal control group, AD model group, HLJDD group (12.8 g/kg), CPF group, 40AEF group, 90AEF group, WEF group, and PEF group. To prepare the 2,4-dinitro-1-fluorobenzene (DNFB) solution, DNFB was dissolved in acetone/olive oil (4:1) and applied to mouse skin. The procedure was performed as previously reported, with some modifications (Chen et al, 2020a). Briefly, an electric shaver was used to remove the hair from the abdominal and back skin of mice on the first day (the area of hair removal was about 2 × 2 cm^2). Then, 200 µl of 1% DNFB was used to sensitize the abdominal skin on days 1, 4, and 7, once a day, for a total of three times. The mice were challenged with 200 µl of 0.5% DNFB on the back skin on days 14, 17, 19, 22, 24, 27, and 29 in the model and HLJDD groups, once a day. Mice from the control group were smeared with an equal volume of DNFB matrix solution at the same time points. After being challenged, the mice from the HLJDD groups and its fractions groups were intragastrically administered with HLJDD (12.8 g/kg) and its fractions (CPF: 921.6 mg/kg, 40AEF: 458.24 mg/kg, 90AEF: 460.8 mg/kg, WEF: 1.0086 g/kg, PEF: 1.38 mg/kg) once a day for 16 days, respectively, while the mice from normal control group and AD model group were administrated with an equal volume of saline. After the last administration, each group of mice was anesthetized. Blood samples were collected from the ophthalmic venous plexus, from which serum was separated and stored at −80°C for future research. Finally, the mice were sacrificed, and the dorsal skin tissue samples were harvested and stored at −80°C for further analysis.

Evaluation of Back Skin Lesions

The AD-like symptoms of skin induced by DNFB were scored upon completion of drug treatment. The back lesions were evaluated based on clinical presentation criteria (Choi et al., 2018): erythema, edema/papules, epidermal stripping/scratches, and scales (dry), which were categorized into four grades: no lesion, light, medium, and severe (recorded as 0, 1, 2, and 3, respectively). Ear thickness was measured using a Vernier caliper, and the difference between the weight of the left and right ears was calculated as the degree of swelling. The swelling rate of the ear was calculated as follows (Li et al., 2020): [(the degree of swelling of ear in AD model group − the degree of swelling of ear after treatment)/the degree of ear swelling in the AD model group] × 100%.

H&E Staining

The dorsal skin was embedded in paraffin and sliced into 5-µm sections. The pathological sections were stained with hematoxylin and eosin (H&E), and the sections were examined under an optical microscope.

Index Measurement

The serum levels of IgE and histamine were determined using the appropriate ELISA kits according to the manufacturer's instructions. The serum levels of IL-13, IL-17A, IL-3, IL-31, IL-33, IL4, IL-5, and TSLP in the serum were measured using Luminex technology (R&D Systems, Abingdon, United Kingdom) on a Luminex 200 instrument.

Real-Time PCR Analysis

RT-PCR was used to determine the expression levels of JAK1, HRH4, and IL-4Rα mRNAs. Total RNA was isolated and extracted from the dorsal skin tissues using TRIzol® reagent (Invitrogen, Thermo Fisher Scientific, Inc.). Reverse transcription was performed to synthesize cDNA using the HiScript II Q RT SuperMix for qPCR (+gDNA wiper) (R223-01; Vazyme, Inc.). RT-PCR analysis was performed using 2× SYBR Green PCR Master Mix (A4004M; Lifeint) on a CFX Connect™ PCR instrument (Bio-Rad Laboratories, Shanghai, China) according to the manufacturer's protocol. The primer sequences were as follows: JAK1 specific primer (forward: 5′-GGCGTTCTGTGCTAAAATGA-3′, reverse: 5′-AGGGCGAAG AGGTTGTGAC-3′), IL-4Rα specific primer (forward: 5′-GGA GGAGGAAGAAGATGAGATAG-3′, reverse: 5′-CCAACAAGT CGGAAAACAGG-3′), HRH4 specific primer (forward: 5′-TGA CTTCCTCGTGGGTTTG-3′, reverse: 5′-ATTGTAGACAGA TGCGGTGC-3′), and β-actin specific primer (forward: 5′-AGGGAAATCGTGCGTGAC-3′, reverse: 5′-CATACCCAA GAAGGAAGGCT-3′). The expression levels of the target mRNAs were calculated based on normalization to β-actin expression.

Western Blot Analysis

Western blotting was performed to evaluate the protein expression of IL-4Rα, JAK1, p-JAK1, and HRH4. Briefly, total protein from dorsal skin tissue was extracted and quantified using the BCA protein quantitative assay. Protein sample buffer was added and heated in a boiling water bath. The denatured protein was separated on a 12% polyacrylamide gel and transferred to a polyvinylidene fluoride membrane.

TABLE 1 | UPLC-Q-TOF/MS identification of the constituents in HLJDD.

NO.	t_R (min)		Positive ion MS	Negative ion MS	Formula	Identifcation	Positive ion MS/MS	Negative ion MS/MS	Relegation
1	0.58	[M-H]⁻	-	191.0558	$C_7H_{12}O_6$	Quinic acid	-	191.0554, 127.0395, 85.0289	Organic acid
2	0.63	[M-H]⁻	-	133.0142	$C_4H_6O_5$	Malic acid	-	115.0030, 71.0134	Amino acid
3	0.63	[M + H]⁺	175.1187	-	$C_6H_{14}N_4O_2$	Arginine	70.0649	-	Amino acid
4	0.65	[M + H]⁺	116.0699	-	$C_5H_9NO_2$	Proline	70.0648	-	Amino acid
5	0.79	[M + H]⁺	182.081	-	$C_9H_{11}NO_3$	Tyrosine	96.0437	-	Amino acid
6	0.81	[M-H]⁻	-	191.0201	$C_6H_8O_7$	Citric acid	-	173.0077, 111.0079. 87.0080	Organic acid
7	0.86	[M + H]⁺	268.1041	-	$C_{10}H_{13}N_5O_4$	Adenosine	136.0310, 119.0341	-	Nitrogen glycosides
8	1.02	[M + H]⁺	132.1011	-	$C_6H_{13}NO_2$	Isoleucine	86.0960, 69.0688	-	Amino acid
9	1.51	[M + H]⁺	139.0384	-	$C_7H_6O_3$	3.4.Dihydroxybenzaldehyde	136.0181, 119.0160, 108.0228. 81.0360	-	Organic acid
10	1.53	[M + H]⁺	166.0859	-	$C_9H_{11}NO_2$	Phenylalanine	120.0801, 103.0534. 91.0538. 77.0380	-	Amino acid
11	1.6	[M + H]⁺	127.0383	-	$C_6H_6O_3$	Maltol	103.0548. 77.0385	-	Saccharides
12	1.64	[M-H]⁻	-	197.0458	$C_9H_{10}O_5$	danshensu	-	179.0351, 135.0453	Organic acid
13	1.71	[M-H]⁻	-	391.1240	$C_{16}H_{24}O_{11}$	Shanzhiside	-	229.0714, 185.0821, 167.0714	Iridoid
14	1.78	[M-H]⁻	-	373.1135	$C_{16}H_{22}O_{10}$	Geniposidic acid	-	211.0611, 149.0609, 123.0446	Iridoid
15	2.21	[M + H]⁺	208.0974	-	$C_{11}H_{13}NO_3$	Hydrastinine	190.086, 175.0612, 147.0432	-	Alkaloids
16	2.28	[M + H]⁺	192.0419	-	$C_{10}H_8O_4$	7,8-Dihydroxy-4-methylcoumarin	175.0386, 147.0428, 119.0482, 91.0543	-	Coumarin
17	2.98	[M + Na]⁺	427.1201	-	$C_{17}H_{24}O_{11}$	Gardenoside	265.0683, 247.0575, 233.6419, 215.0310	-	Iridoid
18	2.33	[M + H]⁺	188.0704	-	$C_{11}H_9NO_2$	3-Indoleacrylic acid	143.0727, 118.0647	-	Organic acid
19	2.33	[M + H]⁺	205.0969	-	$C_{11}H_{12}N_2O_2$	Tryptophan	188.0694	-	Amino acid
20	2.41	[M + H]⁺	272.1279	-	$C_{16}H_{17}NO_3$	Higenamine	255.1015, 161.0590, 107.0488	-	Alkaloids
21	2.67	[M-H]⁻	-	153.0194	$C_7H_6O_4$	Gentisic acid	-	108.0229. 81.0348. 53.0394	Organic acid
22	2.89	[M-H]⁻	-	369.1516	$C_{16}H_{26}O_8$	Jasminoside B	-	339.1420	Monoterpenoids
23	2.9	[M + H]⁺	355.102	353.0874	$C_{16}H_{18}O_9$	Chlorogenic acid	163.0380, 145.0279, 135.0437	353.0874, 91.0561, 179.0358, 35.0448	Organic acid
24	3.09	[M + Na]⁺	395.1305	-	$C_{17}H_{24}O_9$	Eleutheroside B	364.1139, 232.0708	-	-
25	3.12	[M-H]⁻	-	353.0873	$C_{16}H_{18}O_9$	4-Ocaffeoylquinic acid	-	353.0877, 173.0454, 135.0446	Organic acid
26	3.28	[M + HCOOH-H]⁻	-	595.1876	$C_{23}H_{34}O_{15}$	Genipin gentiobioside	-	517.1567, 323.0988, 225.0769, 207.0663	Iridoid
27	3.29	[M + Na]⁺	573.1782	-	$C_{23}H_{34}O_{15}$	Genipin-1-gentiobioside	541.1509, 511.1411, 365.1031, 347.0937, 305.0835	-	Iridoid
28	3.38	[M + Na]⁺	411.1264	-	$C_{17}H_{24}O_{10}$	Geniposide[a]	379.0960, 349.0902, 249.0728, 231.0618,217.0467, 203.0527, 185.0415, 147.0411	-	Iridoid
29	3.76	[M + H]⁺	169.0755	-	$C_{11}H_8N_2$	Norharmane	115.0539	-	-
30	3.77	[M-H]⁻	-	341.1622	$C_{20}H_{24}NO_4$	Phellodendrine	-	-	Alkaloids
31	4.8	[M + H]⁺	195.0657	-	$C_{10}H_{10}O_4$	Ferulic Acid[a]	145.0279, 117.0326. 89.0379	-	Organic acid
32	5.14	[M + NH₄]⁺	207.0646	-	$C_{11}H_{12}O_5$	3,5-Dimethoxy-4-hydroxycinnamic acid	192.0410, 147.0445, 119.0498	-	Organic acid
33	5.18	[M + H]⁺/[M-H]⁻	611.1601	609.1458	$C_{27}H_{30}O_{16}$	Rutin	303.0491	-	Flavonoid
34	5.18	[M + H]⁺	303.0494	-	$C_{15}H_{10}O_7$	Quercetin	-	285.0409, 257.0419, 229.0484	Flavonoid
35	4.8	[M + H]⁺	322.1069	-	$C_{19}H_{15}NO_4$	Berberrubine	307.0814, 294.1114, 279.0865	-	Alkaloids

(Continued on following page)

TABLE 1 | (Continued) UPLC-Q-TOF/MS identification of the constituents in HLJDD.

NO.	t_R (min)		Positive ion MS	Negative ion MS	Formula	Identifcation	Positive ion MS/MS	Negative ion MS/MS	Relegation
36	5.54	[M + H]$^+$	509.1281	-	$C_{23}H_{24}O_{13}$	Syringetin 3-glucoside	347.0758, 332.0528	-	Phenylethanoid glycoside
37	5.76	[M + H]$^+$	352.1174	-	$C_{20}H_{17}NO_5$	8-O-berberine	337.0929, 308.0900	-	Alkaloids
38	5.78	[M-H]$^-$	-	515.1188	$C_{25}H_{24}O_{12}$	Isochlorogenic acid A[a]	-	-	Organic acid
39	5.83	[M + H]$^+$	356.1846	-	$C_{21}H_{25}NO_4$	Tetrahydropalmatine	192.1004, 177.0770, 165.0915	-	Alkaloids
40	5.89	[M-H]$^-$	-	623.1974	$C_{29}H_{36}O_{15}$	Methyl hesperidin	-	461.1673, 415.1035, 295.0622, 161.0248	Flavonoid
41	5.99	[M + H]$^+$	354.1337	-	$C_{20}H_{19}NO_5$	Protopine[a]	-	-	Alkaloids
42	6.14	[M]$^+$	336.1221	-	$C_{20}H_{18}NO_4$	Epiberberine	320.0892, 292.0942	-	Alkaloids
43	6.25	[M]$^+$	338.1393	-	$C_{20}H_{20}NO_4$	Dihydroberberine	322.1048, 294.1098	-	Alkaloids
44	6.28	[M]$^+$	461.1071	-	$C_{22}H_{21}O_{11}$	Oroxylin A 7-O-glucuronide	285.0761, 270.0530	-	Flavonoid
45	6.28	[M + H]$^+$	523.1435		$C_{24}H_{26}O_{13}$	Iridin	361.0900, 331.0438	-	Flavonoid
46	6.35	[M]$^+$	320.0913	-	$C_{19}H_{14}NO_4$	Coptisine	292.0592	-	Alkaloids
47	6.53	[M]$^+$	352.1197	-	$C_{21}H_{22}NO_4$	Palmatine[a]	336.1232, 308.1289	-	Alkaloids
48	6.71	[M]$^+$	336.1222	-	$C_{20}H_{18}NO_4$	Berberine[a]	320.0876, 306.0749, 304.0956, 292.0942, 278.0787	-	Alkaloids
49	6.8	[M + H]$^+$	463.0861	-	$C_{21}H_{18}O_{12}$	Scutellarin	287.0548, 269.0444, 241.0488	-	Flavonoid
50	6.88	[M + H]$^+$	417.1173	-	$C_{21}H_{20}O_9$	Chrysin 8-C-glucopyranoside	399.1088, 297.0758, 267.0653	-	Flavonoid
51	7.08	[M + H]$^+$	273.0748	-	$C_{15}H_{12}O_5$	Dihydronorwogonin	169.0124	-	Flavonoid
52	7.17	[M + H]$^+$	447.0917	-	$C_{21}H_{19}O_{11}$	Baicalin[a]	271.0581, 169.0123	-	Flavonoid
53	7.22	[M + H]$^+$	593.1871	-	$C_{28}H_{32}O_{14}$	Linarin	447.1269, 285.0755	-	Flavonoid
54	7.42	[M-H]$^-$	-	459.0923	$C_{22}H_{20}O_{11}$	Wogonoside[a]	-	459.0907, 268.0370, 239.0349	Flavonoid
55	7.46	[M-H]$^-$	-	429.0816	$C_{21}H_{18}O_{10}$	Chrysin-7-O-β-d-glucuronide	-	253.0508, 175.0249, 113.0255	Flavonoid
56	7.6	[M-H]$^-$	-	475.0874	$C_{22}H_{20}O_{12}$	Hydroxyl oroxylin A-7-O-β-d-glucutonide		299.0555, 284.0316, 255.0298,175.0246, 113.0241	Flavonoid
57	7.75	[M-H]$^-$	331.0806	-	$C_{17}H_{14}O_7$	5, 7, 4' -trihydroxy-3 ', 5' -dimethoxy flavone	-	316.0588, 270.0507	Flavonoid
58	8.02	[M-H]$^-$	-	299.0555	$C_{16}H_{12}O_6$	Hispidulin		284.0342, 269.0359, 239.0371, 136.9880	Flavonoid
59	8.26	[M + H]$^+$	260.0906	-	$C_{14}H_{13}NO_4$	Skimmianine	245.0663, 227.0557	-	Alkaloids
60	8.49	[M-H]$^-$	-	975.3713	$C_{44}H_{64}O_{24}$	Crocin	-	651.2661, 327.1600	Flavonoid
61	9.2	[M-H]$^-$	-	299.0557	$C_{16}H_{12}O_6$	4 -Hydroxywogonina	-	284.0342, 239.0372,136.9880	Flavonoid
62	9.28	[M]$^+$	470.1962	-	$C_{26}H_{30}O_8$	Obaculactone	425.1936, 409.2004	-	-
63	9.66	[M + H]$^+$	375.1045	-	$C_{19}H_{18}O_8$	Casticin	375.0572	-	-
64	9.72	[M + H]$^+$	285.0748	283.0612	$C_{16}H_{12}O_5$	Wogonin[a]	270.0502	283.0608, 163.0027	Flavonoid
65	9.81	[M + H]$^+$	255.0638	253.0506	$C_{15}H_{10}O_4$	Chrysin[a]	-	209.0616 183.0472, 143.0509, 107.0143	Flavonoid
66	9.88	[M + H]$^+$	315.0852	-	$C_{17}H_{14}O_6$	3,7-Dihydroxy-3′,4′-dimethoxyflavone	300.0613, 285.0372, 257.0426	-	-
67	10.28	[M-H]$^-$	-	343.0818	$C_{18}H_{16}O_7$	5, 7-dihydroxy-2 ',6 ', 8-trimethoxylflavone	-	313.0351, 285.0405, 269.0402	Flavonoid
68	10.39	[M + H]$^+$	286.1431	-	$C_{17}H_{19}NO_3$	Piperine	-	-	Alkaloids
69	10.5	[M + H]$^+$	455.2051	-	$C_{26}H_{30}O_7$	Obacunone[a]	437.1929, 409.2004	-	Flavonoid
70	10.32	[M + H]$^+$	288.1585	-	$C_{18}H_{13}N_3O$	Rutecarpine[a]	-	-	Alkaloids
71	12.49	[M + H]$^+$	299.1604	-	$C_{19}H_{22}O_3$	Auraptene[a]	-	-	Flavonoid
72	18.82	[M + H]$^+$	397.3814	-	$C_{29}H_{50}O$	β-Sitosterol	147.123	-	Sterols

[a]Indicates comparison with reference substance.

The blot was blocked in 5% skimmed milk at room temperature for 2 h, followed by co-incubation with the appropriate proportions of primary and secondary antibodies. The number of target bands was detected using ECL chemiluminescence. The antibodies used for western blotting were anti-IL-4Rα (#DF8567; Affinity), anti-JAK1

(#66466-1-ap; Proteintech), anti-p-JAK1 (#AF 2012; Affinity), and anti-HRH4 (#OM209489; Omnimabs).

Untargeted Metabolomics

To explore the changes in the metabolomic characteristics of AD, the concentrations of different serum metabolites in AD and HLJDD-treated mice were confirmed by a UPLC-Q-TOF/MS/MS-based metabolomic approach. Details of chromatography, mass spectrometry conditions, and data processing are provided in **Supplementary Material S5**.

Targeted Metabolomics

To screen for discriminatory metabolites, Pearson's correlation analysis was performed to analyze the correlation between macroscopic indexes and metabolites. Metabolites significantly associated with macroscopic indices were used to further evaluate the mechanism of HLJDD fractions. Meanwhile, considering the accuracy of metabolites and the diversity detected in each sample, we performed a targeted quantification of 14 endogenous metabolites (targeted metabolomics). The standard substances (prostaglandin D1, phosphocreatinine, n-methyl-d-aspartic acid, n-hydroxymethylnorcotinine, malic acid, lysopc (24:1 (15z)), linolelaidic acid, l-alloisoleucine, l-alanine, humulinone, glutaric acid, gamma-linolenic acid, dihydro-o-methylsterigmatocystin, deoxyuridine, d-phenyllactic acid, carnosine, biliverdin, alanyl-glutamine, 4-imidazolone-5-propionic acid, 3,7-dimethylpurine-2,6-dione, 2-hydroxy-2-methylbutanedioic acid, 1h-pyrimidine-2,4-dione, and (z)-tetracos-15-enoic acid) were dissolved in a diluent (methanol/acetonitrile = 1:1) for further study.

Details of sample processing, chromatography, mass spectrometry conditions, and data processing are described in **Supplementary Material S6**, and the MRM parameters of standard substances are given in **Supplementary Table S1**.

Furthermore, receiver operating characteristic (ROC) curve analysis and area calculation curve (AUC) under ROC were performed to evaluate the change in the diagnostic ability of potential biomarkers.

Statistical Analysis

All values are presented as the mean ± standard deviation (SD). The significance of differences among the groups was determined by one-way analysis of variance (ANOVA) using the statistical package for the social science program (SPSS 19.0, Chicago, IL, United States). Statistical significance was set at $p < 0.05$.

RESULTS AND DISCUSSION

Splitting HLJDD Fractions and Establishment of HPLC Fingerprints

HLJDD was split into five fractions: CPF (yield, 7.200 ± 0.731%, $n = 5$), PEF (yield, 0.0108 ± 0.002%, $n = 5$), 40AEF (yield, 3.580 ± 0.179%, $n = 5$), 90AEF (yield, 3.60 ± 0.752%, $n = 5$), and WEF (yield, 7.880 ± 0.928%, $n = 5$). The HPLC fingerprints of four fractions (WEF, 40AEF, 90AEF, and PEF) were successfully

established, and the similarity of eight batches of samples was above 0.9, suggesting that the stability of the process was relatively good (**Supplementary Figures S1–S4**).

Qualitative Analysis by UPLC-Q-TOF/MS

According to the analysis of the mass fragment information of each chemical component in the Massbank database, 72 chemical components were identified and compared with the literature data. Among these major constituents, 15 alkaloids, 22 flavonoids, 6 iridoids, 18 organic acids and amino acids, and 11 other constituents were identified in this experiment (**Table 1**).

Alkaloids

Coptis chinensis Franch. and *Phellodendron amurense* Rupr. were found to be the main drugs of HLJDD, and contained large quantities of alkaloids, including coptisine, palmatine, and berberine. These ingredients of HLJDD exhibit a wide range of pharmacological effects and biological activities (Chen et al., 2020a). A total of 15 alkaloid chemical components (compound 15, 20, 30, 35, 37, 39, 41-43, 46-48, 59, 66, and 70) were identified in this study: hydrastinine, higenamine, phellodendrine, berberrubine, 8-O-berberine, tetrahydropalmatine, protopine, epiberberine, dihydroberberine, coptisine, palmatine, berberine, skimmianine, piperine, and rutecarpine. Berberine was used an example to evaluate the possible cleavage pathway of alkaloids. Compound 48 was determined as berberine using pure standard data and combining the fragmentation rules with data reported in the literature. First, berberine showed fragment ions at m/z 336.1222 $[M]^+$, 320.0876 $[M-CH_4]^+$, 306.0749 $[M-CH_4-CH_2]^+$, 292.0942 $[M-CH_4-CO]^+$, and 278.0787 $[MCH_4-CO-CH_2]^+$. The fragmentation at m/z 320.0876 $[M-CH_4]^+$ was acquired at m/z 336.1222 $[M]^+$ through the loss of a molecule of CH_3 and a rearrangement reaction. Further, this fragmentation lost the methyl group at the end site to form fragment ions at m/z 306.0749 $[M-CH_4-CH_2]^+$; on the other hand, this fragmentation also resulted in the formation fragment ions at m/z 292.0942 $[M-CH_4-CO]^+$ by the cracking of the side benzene ring and the loss of a molecule of CO, and continued to lose of the side ring-CH_2 fragment and formed fragment ions at m/z 278.0787 $[MCH_4-CO-CH_2]^+$. Combined with standard substance analysis and the literature (Zuo et al., 2014) this was inferred as berberine (**Supplementary Figure S5**).

Flavonoids

Flavonoids are the main active components in the form of either sugar glucoside or free molecules in natural plants. They possess many bio-activities, including lipid-lowering (Yao et al., 2014), antitumor (Wang et al., 2020), anti-oxidation (Wang et al., 2021), and anti-bacterial (Rasouli et al., 2019). Scutellariae Radix in HLJDT contains a large amount of flavonoids, such as quercetin, rutin, baicalin, wogonin, and chrysin (Yang et al., 2020). A total of 22 flavonoids (compound 33-34, 40, 44-45, 49-58, 60-61, 64-65, 67, 69, and 71) were identified in this study: rutin, quercetin, methyl hesperidin, oroxylin A 7-O-glucuronide, iridin, scutellarin, chrysin 8-C-glucopyranoside, dihydronorwogonin, baicalin, linarin, wogonoside, chrysin-7-O-β-d-glucuronide,

Hydroxyl oroxylin A-7-O-β-d-glucutonide, 5,7,4′-trihydroxy-3′, 5′-dimethoxy, hispidulin, crocin, 4-hydroxywogonina, wogonin, chrysin, 5, 7-dihydroxy-2′,6′, 8-trimethoxylflavone, obacunone, and auraptene. Of these, baicalin, wogonoside, wogonin, chrysin, obacunone, and auraptene were identified using pure standards. Flavonoids often exist in the form of flavonoid glycosides. Therefore, the fragmentation regularity of flavonoids mainly includes the breakage of glycosidic bonds and flavonoid aglycon (Ferreres et al., 2004). For example, in the positive ion mode, baicalin (compound 19), excimer ions broke the glycosidic bond and formed fragment ions at m/z 271.0581 [M + H-GlucA]$^+$. Furthermore, the flavonoid aglycon was opened and cleaved to m/z 169.0123 [M + H-GlucA-C_7H_2O]$^+$. The mass spectrometry cleavage pathway is illustrated in **Supplementary Figure S6**.

Iridoids

Iridoids mainly come from gardeniae fructus and have hypoglycemic, anti-inflammatory, and anti-tumor effects (Hung et al., 2010; Koo et al., 2004; Xu and Hao, 2004). A total of six iridoids (compounds 13, 14, 17, 26, 27, and 28) were identified in this study. These were shanzhiside, geniposidic acid, gardenoside, genipin gentiobioside, genipin-1-gentiobioside, and geniposide by combining the fragmentation rules with data from the literature. Geniposide was identified using a standard. For example, the mass spectrometry cleavage pathway of geniposide (compound 28) is shown in **Supplementary Figure S7**. The molecular ion peak of m/z 411.1264 [M + Na]$^+$ was obtained in positive mode, and hydrogen on the double bond appeared lively due to the influence of oxygen atoms, combining with the oxygen on the ester bond. After fracturing, the mother nucleus lost a molecule of CH_3OH to form a fragment ion at m/z 379.0960, which continued to lose glucose or formaldehyde molecules to form fragment ions at m/z 217.0467 or 349.0902. The glycosidic bond of geniposide has two cleavage pathways. On the one hand, active hydrogen on the mother nucleus transferred and formed fragment ions at m/z 231.0618 and complete glucose fragment ions at m/z 203.0527. On the other hand, the active hydrogen on the glucose transferred and formed fragment ions at m/z 249.0728 and complete glucose fragment ions at m/z 185.0415. In summary, combined with standard substances and the literature, it was inferred as geniposide (Zuo et al., 2014).

Organic Acids and Amino Acid

Many organic acid compounds are mainly classified into small molecule phenolic acid compounds and acylated organic acid compounds according to their structure (Krzymińska et al., 2020). A total of 18 organic acid and amino acid chemical components (compound 1-6, 8-10, 12, 18-19, 21, 23, 25, 31-32, and 70) were identified in this study: quinic acid, malic acid, arginine, proline, tyrosine, citric acid, isoleucine, 3,4-dihydroxybenzaldehyde, phenylalanine, danshensu, 3-indoleacrylic acid, tryptophan, 3,5-dimethoxy-4-hydroxycinnamic acid, gentisic acid, chlorogenic acid, 4-ocaffeoylquinic acid, ferulic acid, and isochlorogenic acid. In negative ion mode, the parent ion of the small-molecule phenolic acid compound easily lost the H_2O and CO_2 groups,

and the acylated organic acid easily produced fragment ions at m/z 191 [$C_7H_{11}O_6$]$^-$, 179 [$C_9H_7O_4$]$^-$, 173 [$C_7H_9O_5$]$^-$, 163 [$C_9H_7O_3$]$^-$, and 135 [$C_8H_7O_2$]$^-$. Similarly, for compound 25, ions at m/z 353.0878 [M-H]$^-$, 335.0730 [M-H-H_2O]$^-$, 191.0558 [M-H-Caffeoyl]$^-$, 179.0348 [M-H-Quinic]$^-$, 173.0454 [M-H-Caffeoyl-H_2O]$^-$, 135.0447 [M-H-Quinic-CO_2]$^-$ were acquired in negative mode, and those at m/z 335.0730 [M-H-H_2O]$^-$, 191.0558 [M-H-Caffeoyl]$^-$, and 179.0348 [M-H-Quinic]$^-$, corresponding to NLs of 18 Da ($H2O$), 162 Da (caffeoyl), 174 Da (quinic), and the parent ion for m/z 353.0878 [M-H]$^-$, were indicative of 4-ocaffeoylquinic acid (Guo et al., 2014), indicating formula $C_{16}H_{18}O_9$. The cleavage pathway is shown in Figure S8.

Others

A total of 11 other components (compounds 7, 11, 16, 22, 24, 29, 36, 62, 63, 66, and 72) were identified in this study: adenosine, maltol, 7,8-dihydroxy-4-methylcoumarin, jasminoside B, eleutheroside B, norharmane, syringetin 3-glucoside, obaculactone, casticin, 3,7-dihydroxy-3′,4′-dimethoxyflavone, and β-sitosterol.

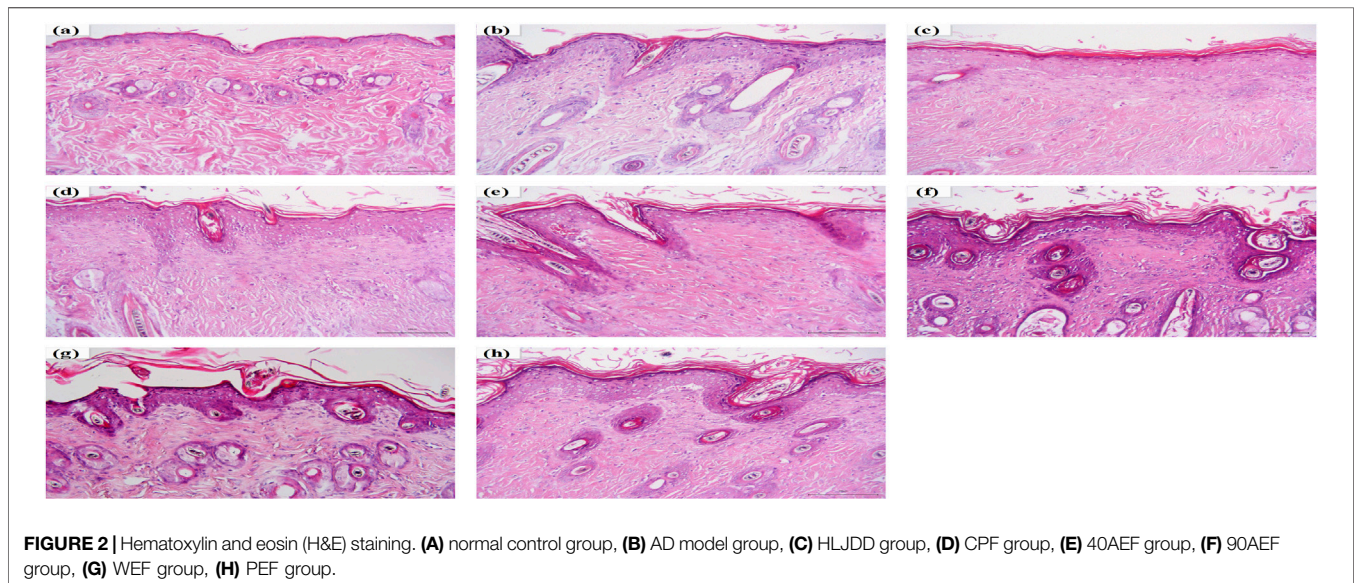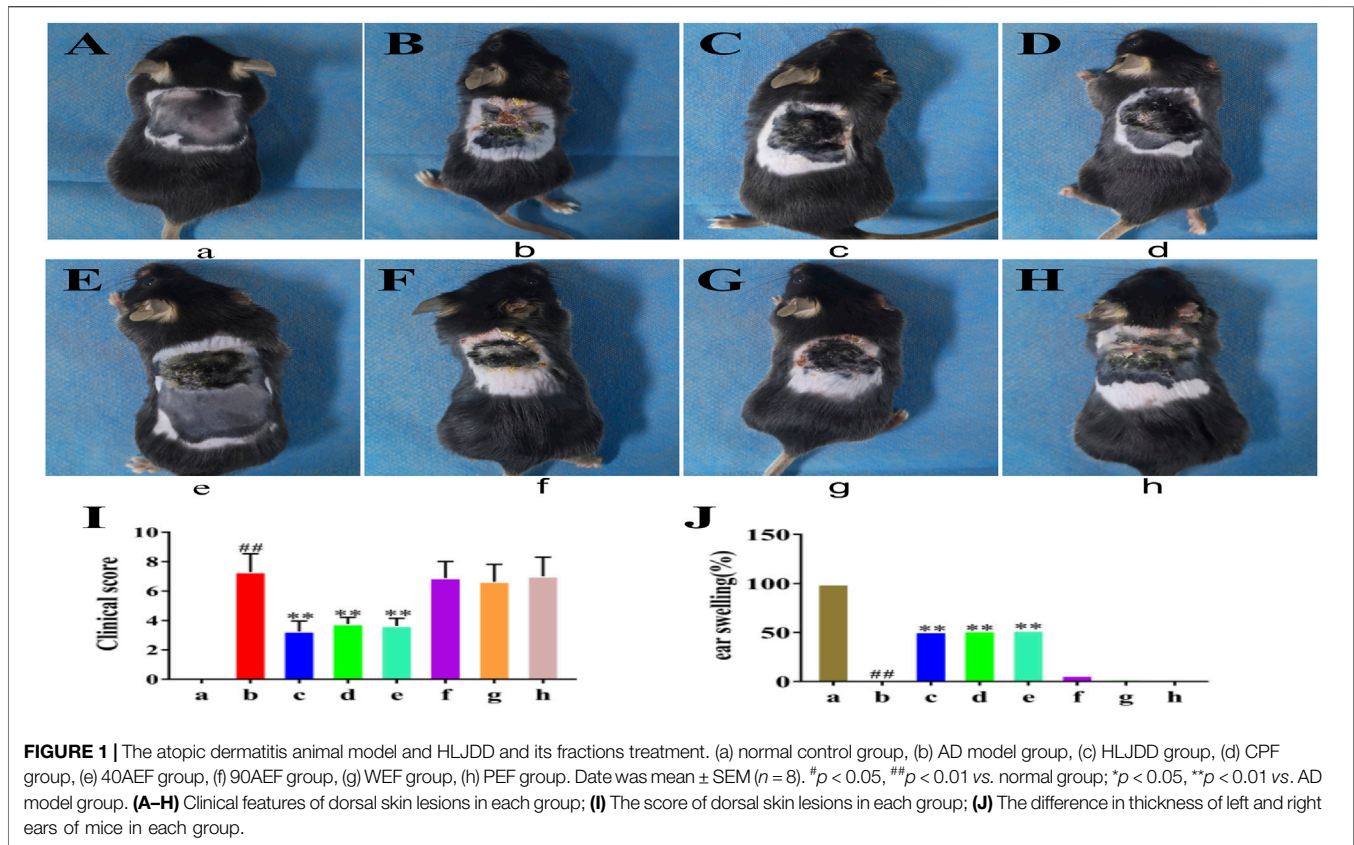# Non-similarity Degree Evaluation of Chemical Fractions

Qualitative Analysis

The accumulative variance contributions of the first three principal components were 94.95% (positive ion mode) and 94.34% (negative ion mode), respectively, indicating that the PCA method achieved a higher recognition rate. As shown in **Supplementary Figure S9A,B**, a clear separation was observed among the four chemical fractions, indicating that the degree of similarity of the chemical fractions was small. Furthermore, HCA was performed using the data of 72 chemical components, and a clear separation was observed among the four chemical fractions as well. In addition, we intuitively understood the main components of the four chemical fractions. As shown in **Supplementary Figure S10**, the main components of 40AEF, 90AEF, PEF, and WEF were alkaloids, flavonoids, and a few alkaloids, iridoids, organic acids, and amino acids.

Quantitative Analysis

Further, the non-similarity degree (NSD) was measured by the cross-analysis of the peak areas of crude drug, angle cosine analysis method, and correlation coefficient analysis method, and was used to quantitatively analyze the non-overlapping property of the chemical fractions. As shown in **Supplementary Table S2**, the results showed that NSD was higher than 96.27% among the different fractions.

In this study, 72 chemical components were identified, and the main components of 40AEF, 90AEF, PEF, and WEF were alkaloids, flavonoids, alkaloids, iridoids, organic acids, and amino acids. Meanwhile, the non-overlapping property of the chemical fractions was measured by cross-analysis of the peak areas of the crude drug, angle cosine analysis method, and correlation coefficient analysis method, which was used to verify the results of the HPLC data. As shown in

FIGURE 1 | The atopic dermatitis animal model and HLJDD and its fractions treatment. (a) normal control group, (b) AD model group, (c) HLJDD group, (d) CPF group, (e) 40AEF group, (f) 90AEF group, (g) WEF group, (h) PEF group. Date was mean ± SEM (n = 8). $^\#p < 0.05$, $^{\#\#}p < 0.01$ $vs.$ normal group; $^*p < 0.05$, $^{**}p < 0.01$ $vs.$ AD model group. **(A–H)** Clinical features of dorsal skin lesions in each group; **(I)** The score of dorsal skin lesions in each group; **(J)** The difference in thickness of left and right ears of mice in each group.

FIGURE 2 | Hematoxylin and eosin (H&E) staining. **(A)** normal control group, **(B)** AD model group, **(C)** HLJDD group, **(D)** CPF group, **(E)** 40AEF group, **(F)** 90AEF group, **(G)** WEF group, **(H)** PEF group.
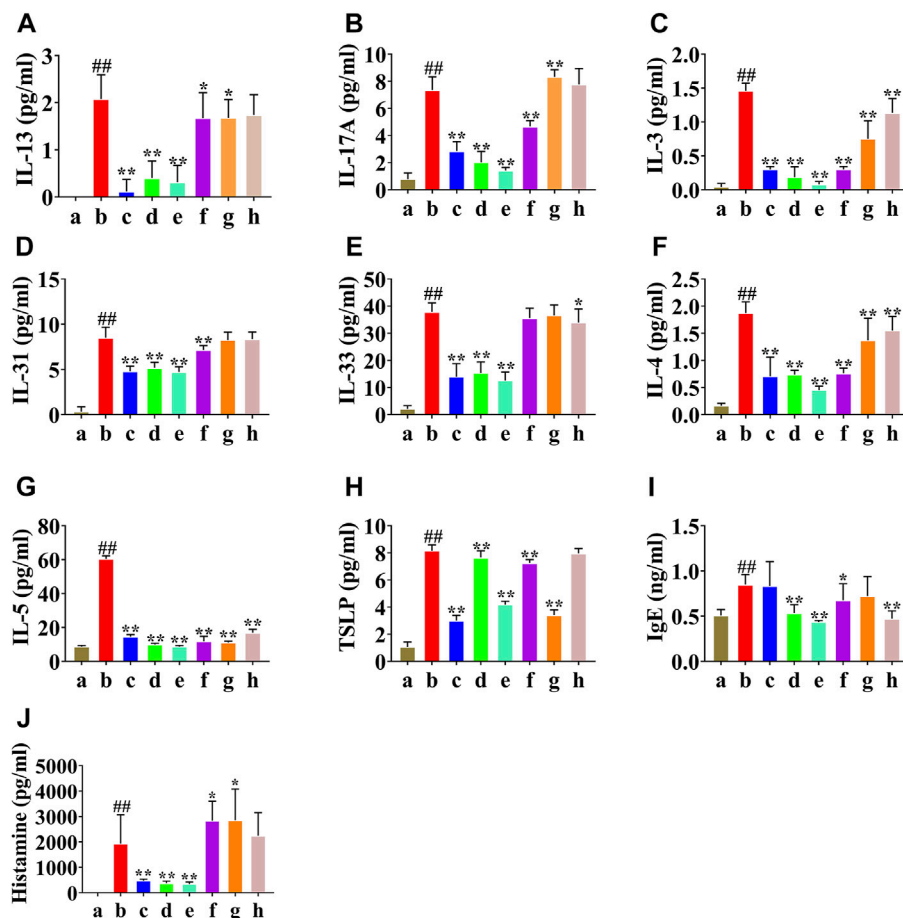
FIGURE 3 | The atopic dermatitis animal model and HLJDD and its fractions treatment (A–J). (a) normal group, (b) AD model group, (c) WD group, (d) CPF (300 mg/kg) group, (e) 40AEF group, (f) 90AEF group, (g) WEF group, (h) PEF group. Date was mean ± SEM (n = 8). ##p < 0.01 vs. normal group; *p < 0.05, **p < 0.01 vs. AD model group.

Supplementary Table S3, the analysis results showed that NSD was higher than 81.00% among the different fractions.
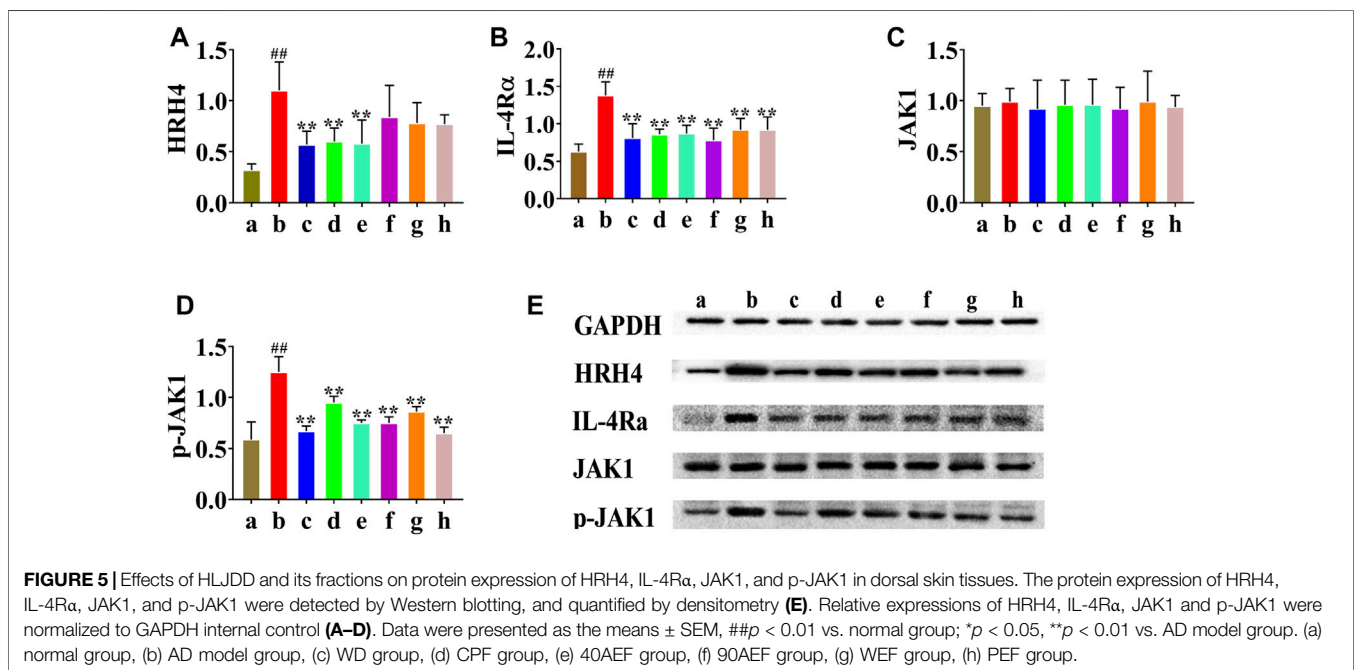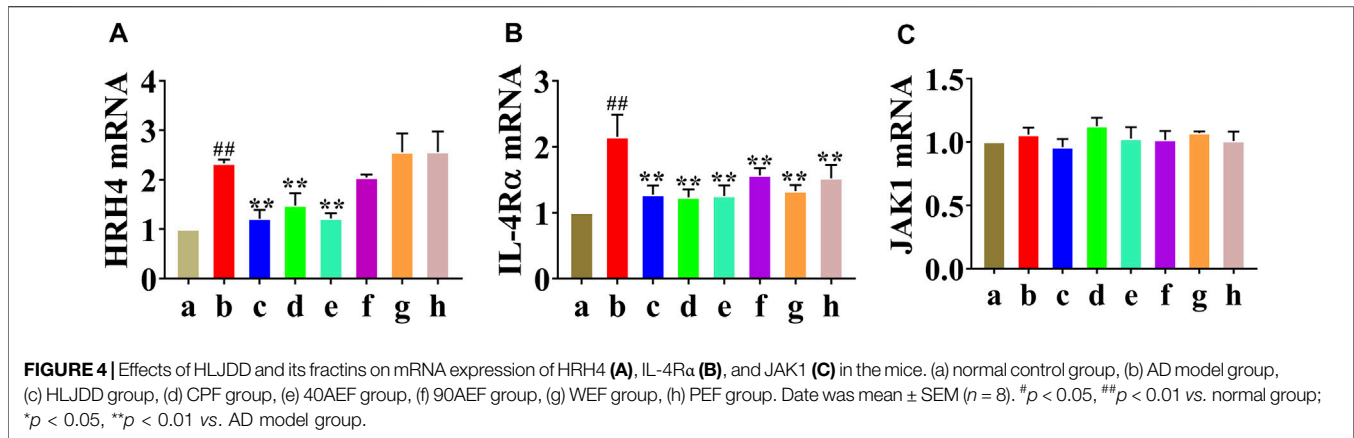
Evaluation of Skin Lesions on AD Mice Model Treated With HLJDD and its Fractions

The AD model was established with DNFB and used to investigate the therapeutic effects of HLJDD (12.8 g/kg) and its fractions (CPF, 40AEF, 90AEF, WEF, and PEF). In comparison with the normal control group, dorsal skin from the AD model group demonstrated severe lesions and showed typical allergic responses, including itching, increased ear and epidermal thickness, swelling, dryness, and erythema. After treatment, the above symptoms in the dorsal skin of mice in the HLJDD group and groups treated with its fractions were remarkably improved (**Figures 1A–H**), especially in the HLJDD, 40AEF, and 90AEF groups. Furthermore, the results of clinical scores indicated that the scores of the AD model group were significantly higher than those of the normal control group, while the HLJDD, CPF, and 40AEF groups showed

significantly lower scores (p < 0.01) (**Figure 1I**). In addition, the inhibitory rate of ear swelling was significantly increased in the HLJDD, CPF, and 40AEF groups compared to the AD model group (**Figure 1J**). These results indicated that HLJDD and its fractions had significant ameliorating effects on AD model mice, especially HLJDD, 40AEF, and CPF.

Histological Examination

To further demonstrate the therapeutic effect of HLJDD and its fractions, we compared the pathology of DNFB-induced skin lesions with or without HLJDD and its fractions (**Figure 2**). In the normal control group, the subcutaneous structure was intact and lined with a thin epithelial layer, showing no signs of inflammatory cell infiltration. In the AD model group, thickening of the epidermis was obvious, where hyperkeratosis and thickening of the spinous cell layer had occurred. Inflammatory cells infiltrating the dermis were also observed in the AD model group. A similar pathology was observed in the 90AEF, WEF, and PEF groups, however, the thickening of epidermis and the infiltration of inflammatory cells were significantly reduced in the HLJDD, CPF, and 40AEF groups,

FIGURE 4 | Effects of HLJDD and its fractins on mRNA expression of HRH4 **(A)**, IL-4Rα **(B)**, and JAK1 **(C)** in the mice. (a) normal control group, (b) AD model group, (c) HLJDD group, (d) CPF group, (e) 40AEF group, (f) 90AEF group, (g) WEF group, (h) PEF group. Date was mean ± SEM ($n = 8$). $^{\#}p < 0.05$, $^{\#\#}p < 0.01$ vs. normal group; $^{*}p < 0.05$, $^{**}p < 0.01$ vs. AD model group.

FIGURE 5 | Effects of HLJDD and its fractions on protein expression of HRH4, IL-4Rα, JAK1, and p-JAK1 in dorsal skin tissues. The protein expression of HRH4, IL-4Rα, JAK1, and p-JAK1 were detected by Western blotting, and quantified by densitometry **(E)**. Relative expressions of HRH4, IL-4Rα, JAK1 and p-JAK1 were normalized to GAPDH internal control **(A–D)**. Data were presented as the means ± SEM, $^{\#\#}p < 0.01$ vs. normal group; $^{*}p < 0.05$, $^{**}p < 0.01$ vs. AD model group. (a) normal group, (b) AD model group, (c) WD group, (d) CPF group, (e) 40AEF group, (f) 90AEF group, (g) WEF group, (h) PEF group.

suggesting that HLJDD, CPF, and 40AEF could indeed improve DNFB-induced skin lesions.
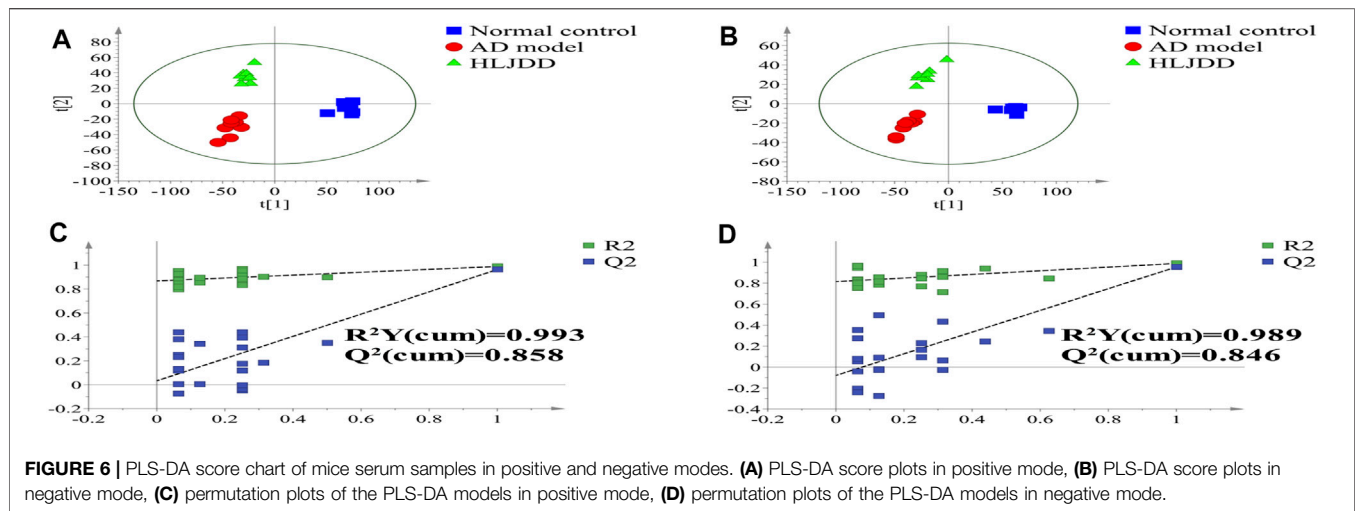
Analysis of HLJDD and its Fractions on Total Serum IgE, Histamine, and Relative Cytokines

To assess the therapeutic effects of HLJDD and its fractions on AD model mice, the total serum IgE and histamine levels were detected by ELISA, and the levels of IL-13, IL-17A, IL-3, IL-31, IL-33, IL4, IL-5, and TSLP were detected using Luminex 200™. The serum IL-13, IL-17A, IL-3, IL-31, IL-33, IL4, IL-5, TSLP, IgE, and histamine levels were significantly increased in the AD model group compared to the normal control group. However, HLJDD markedly decreased serum IL-13, IL-17A, IL-3, IL-31, IL-33, IL4, IL-5, TSLP, and histamine levels; CPF and 40AEF markedly

decreased serum IL-13, IL-17A, IL-3, IL-31, IL-33, IL4, IL-5, TSLP, IgE, and histamine levels; 90AEF markedly decreased serum IL-13, IL-17A, IL-3, IL-31, IL4, IL-5, TSLP, IgE, and histamine levels; WEF markedly decreased serum IL-13, IL-17A, IL-3, IL4, IL-5, TSLP, and histamine levels; PEF markedly decreased serum IL-3, IL-33, IL4, IL-5, and IgE levels. These results indicate that HLJDD and its fractions (especially HLJDD, 40AEF, and 90AEF) had significant ameliorating effects on AD model mice by downregulating the total serum IgE, histamine, and relative cytokines (**Figures 3A–J**).

The Effect of HLJDD and its Fractions on HRH4, IL-4Rα, and JAK1 mRNA Levels

Real-time PCR analysis was performed to examine whether HLJDD affected HRH4, IL-4Rα, and JAK1 mRNA expression.

FIGURE 6 | PLS-DA score chart of mice serum samples in positive and negative modes. **(A)** PLS-DA score plots in positive mode, **(B)** PLS-DA score plots in negative mode, **(C)** permutation plots of the PLS-DA models in positive mode, **(D)** permutation plots of the PLS-DA models in negative mode.

As shown in **Figure 4A**, the relative content of HRH4 mRNA in the AD model group was increased compared to that in the normal control group ($p < 0.01$), and the HLJDD, CPF, and 40AEF groups were significantly decreased compared with the AD model group ($p < 0.01$). As illustrated in **Figure 4B**, the relative content of IL-4Rα mRNA in the AD model group was increased compared to that in the normal control group ($p < 0.01$), and the HLJDD, CPF, 40AEF, 90AEF, WEF, and PEF groups were significantly decreased compared with the AD model group ($p < 0.01$). However, as illustrated in **Figure 4C**, HLJDD and its fractions did not show an inhibitory effect on the expression of JAK1 mRNA.

HLJDD and its Fractions Decreased HRH4, IL-4Rα, and JAK1 Protein Expression in AD Model Mice

In addition, HRH4, IL-4Rα, JAK1, and p-JAK1 protein expression was detected by western blotting. As shown in **Figures 5A–E**, HRH4, IL-4Rα, and p-JAK1 protein expression was significantly upregulated in the AD model group ($p < 0.01$). After treatment, HLJDD, CPF, and 40AEF significantly reduced the levels of HRH4, IL-4Rα, and p-JAK1 ($p < 0.01$), and 90AEF, WEF, and PEF significantly reduced the levels of IL-4Rα and p-JAK1 ($p < 0.01$). Interestingly, there were no significant changes in the protein expression of JAK1.

Untargeted Metabolomics
PLS-DA Analysis
To identify chemical differences between high-dimensional mass spectra data measured for different groups, we used partial least squares discrimination analysis (PLS-DA) to evaluate the metabolomics datasets. In the PLS-DA analysis, for the positive ion mode, R^2Y (cum) = 0.993 and Q^2 (cum) = 0.858; for the negative ion mode, R^2Y (cum) = 0.989 and Q^2 (cum) = 0.846. Both R^2 and Q^2 exceeded 0.5, indicating that the statistical model had a good fit and predictive ability. There were differences between the three

major clusters: the AD model group was set aside from the normal group and the HLJDD group (**Figures 6A–D**). Therefore, the metabolite profiles were distinctively altered by treatment with HLJDD, suggesting that HLJDD can be an effective treatment for AD. This result is also consistent with the experimental data, where HLJDD showed significant therapeutic efficacy in AD models. Additionally, we observed that the metabolite profile of the control group was very different from that of the model group, suggesting that AD may have caused irreversible metabolic disorders in animals.

Identification of Potential Biomarkers
Biomarkers were screened according to a threshold of variable importance in the projection (VIP) value (VIP > 1) that was generated after PLS-DA processing. The p-value for significantly differential metabolites was set to 0.05. According to the above criteria, 40 significant biomarkers were identified and selected for further study (**Table 2**). Compared with normal control group, the levels of 25 metabolites (L-alloisoleucine, 2-hydroxy-2-methylbutanedioic acid, linolelaidic acid, (2S)-2-aminopentanedioic acid, L-alanine, carnosine, (Z)-tetracos-15-enoic acid, malic acid, gamma-linolenic acid, octadecanedioic acid, (5Z,8Z,11Z,14Z,16E)-18-hydroxyicosa-5,8,11,14,16-pentaenoic acid, D-phenyllactic acid, deoxyuridine, 2-(5-hydroxy-1H-indol-3-yl)acetic acid, orotic acid, prostaglandin D1, N′-hydroxymethylnorcotinine, biliverdin, lysoPE (20:4 (8Z,11Z,14Z,17Z)/0:0), N-[(3R,4R,5S,6R)-2,4,5-trihydroxy-6-(hydroxymethyl)oxan-3-yl]acetamide, N-a-acetyl-L-arginine, L-hypoglycin A, dihydro-O-methylsterigmatocystin, 6-lactoyltetrahydropterin, and phosphocreatinine) were significantly upregulated and 15 metabolites (N-methyl-D-aspartic acid, 3,7-dimethylpurine-2,6-dione, indole-3-propionic acid, 1H-pyrimidine-2,4-dione, docosahexaenoic acid, L-glutamic acid, gamma-glutamylvaline, lysoPC(24:1 (15Z)), humulinone, 4-imidazolone-5-propionic acid, alanyl-glutamine, PC(P-18:1 (11Z)/20:5 (5Z,8Z,11Z,14Z,17Z)), cytosine, glutaminylphenylalanine, and gamma-glutamylleucine)) were

TABLE 2 | Mass databases of 40 potential differential metabolites.

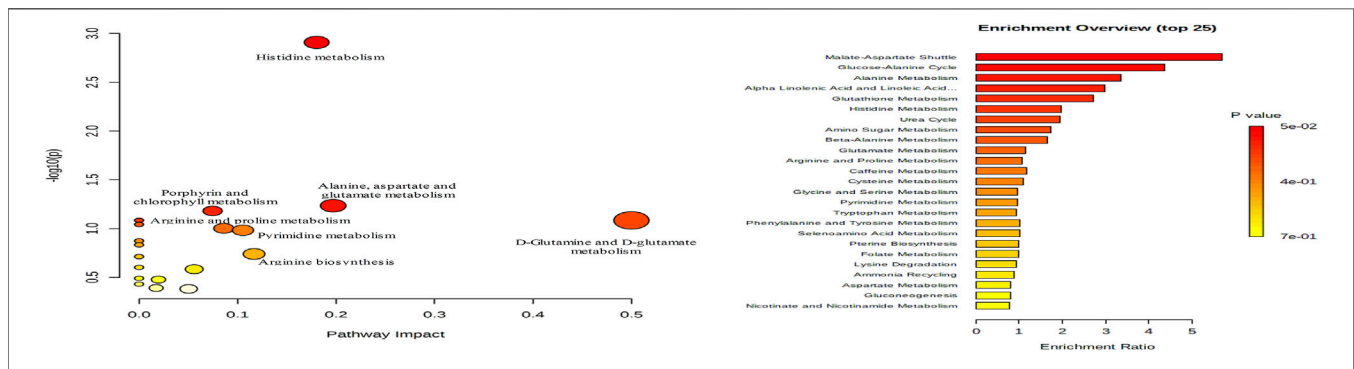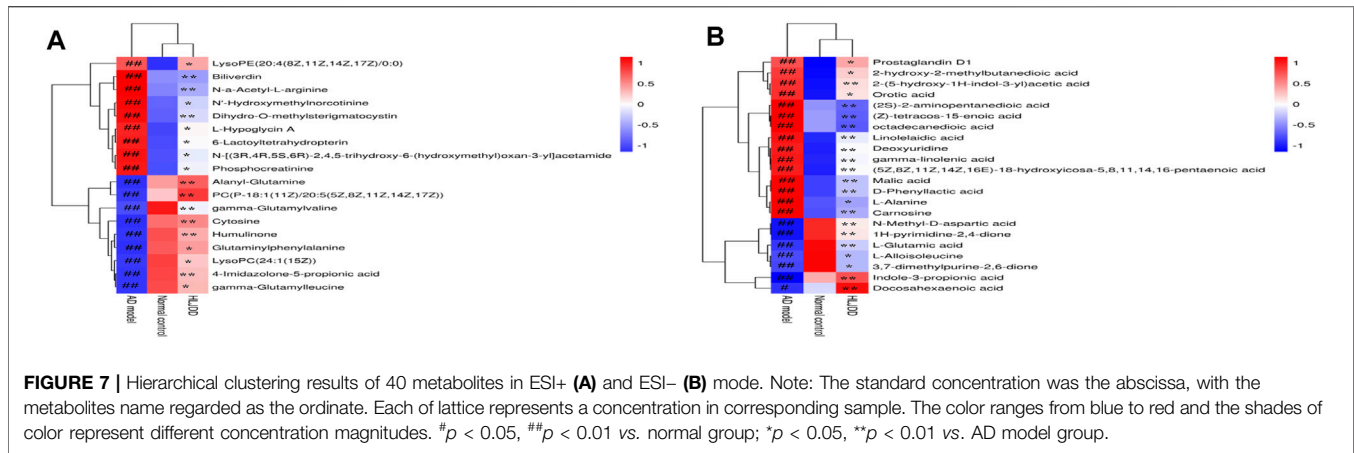| No	R.T.(s)	m/z	Ion mode	Identification results (MS2)	Control group (peak area abundance)	Model group (peak area abundance)	HJDD (peak area abundance)	VIP
1	311.56	131.0356	N	L-Alloisoleucine	14.21 ± 2.31	6.43 ± 1.7##	8.39 ± 1.29*	1.19
2	353.64	146.0824	N	2-hydroxy-2-methylbutanedioic acid	3.1 ± 0.92	5.67 ± 0.67##	4.83 ± 0.56*	1.19
3	45.51	279.2325	N	Linolelaidic acid	384.69 ± 50.49	674.06 ± 65.02##	512.09 ± 133.43**	1.19
4	404.55	146.0460	N	(2S)-2-aminopentanedioic acid	42.57 ± 4.46	50.39 ± 9.34##	41.51 ± 6.68**	1.24
5	349.66	88.0420	N	L-Alanine	21.34 ± 3.27	28.47 ± 5.13##	22.66 ± 5.56*	1.30
6	384.33	226.0482	N	Carnosine	0.95 ± 0.16	1.82 ± 0.1##	1.14 ± 0.32**	1.32
7	313.56	146.0461	N	N-Methyl-D-aspartic acid	22.14 ± 3.37	13.39 ± 1.49##	18.32 ± 4.08**	1.04
8	272.39	179.0558	N	3,7-dimethylpurine-2,6-dione	39.29 ± 9.98	15.91 ± 4.57##	22.15 ± 6.17*	1.14
9	26.91	365.0324	N	(Z)-tetracos-15-enoic acid	7.56 ± 4.22	13.47 ± 2.94##	6.51 ± 1.58**	1.15
10	423.32	132.0308	N	Malic acid	1.62 ± 0.68	6.15 ± 2.29##	2.98 ± 1.04**	1.27
11	95.55	187.1338	N	Indole-3-propionic acid	6.53 ± 2.11	3.67 ± 2.9##	7.32 ± 3.14**	1.06
12	324.89	110.0991	N	1H-pyrimidine-2,4-dione	0.44 ± 0.07	0.16 ± 0.08##	0.32 ± 0.15**	1.34
13	45.69	278.2204	N	γ-Linolenic acid	11.87 ± 2.45	23.29 ± 3.3##	17.32 ± 6.13**	1.13
14	98.97	327.1076	N	Docosahexaenoic acid	6.52 ± 2.9	3.91 ± 1.13#	10.94 ± 4.37**	1.38
15	384.81	131.0547	N	L-Glutamic acid	3.84 ± 0.63	1.53 ± 0.8##	2.32 ± 0.3**	1.23
16	77.65	313.2376	N	octadecanedioic acid	5.46 ± 1.24	9.35 ± 4.51##	4.71 ± 1.19**	1.17
17	39.25	317.1903	N	(5Z,8Z,11Z,14Z,16E)-18-hydroxyicosa-5,8,11,14,16-pentaenoic acid	0.24 ± 0.14	1.31 ± 0.53##	0.76 ± 0.27**	1.28
18	109.13	165.0145	N	D-Phenyllactic acid	3.62 ± 1.47	9.1 ± 3.46##	5.23 ± 3.09**	1.17
19	151.45	226.1446	N	Deoxyuridine	1.84 ± 0.36	5.41 ± 0.99##	3.61 ± 1.61**	1.22
20	186.79	189.0665	N	2-(5-hydroxy-1H-indol-3-yl)acetic acid	0.38 ± 0.11	2.69 ± 0.97##	1.8 ± 0.72**	1.13
21	244.55	155.0102	N	Orotic acid	2.55 ± 0.71	7.55 ± 3.37##	5.49 ± 1.99*	1.39
22	115.78	353.2324	N	Prostaglandin D1	3.53 ± 1.82	19.11 ± 3.56##	15.88 ± 1.96*	1.26
23	405.92	246.1332	P	gamma-Glutamylvaline	3.93 ± 0.99	2.01 ± 0.54##	2.89 ± 0.46**	1.23
24	189.75	606.4496	P	LysoPC(24:1 (15Z))	9.97 ± 0.72	7.93 ± 1.49##	9.34 ± 1.06*	1.32
25	294.90	192.9058	P	N'-Hydroxymethylnorcotinine	2.35 ± 0.25	3.28 ± 0.65##	2.64 ± 0.2*	1.05
26	204.67	582.3182	P	Biliverdin	1.64 ± 0.33	2.72 ± 0.36##	1.68 ± 0.37**	1.24
27	403.25	287.1212	P	Humulinone	4.59 ± 0.63	2.58 ± 0.63##	4.15 ± 0.96**	1.37
28	373.29	157.0599	P	4-Imidazolone-5-propionic acid	17.26 ± 2.67	9.13 ± 2.32##	15 ± 2.76**	1.36
29	203.46	502.2923	P	LysoPE (20:4 (8Z,11Z,14Z,17Z)/0:0)	42.07 ± 12.12	174.45 ± 19.51##	148.54 ± 21**	1.34
30	282.69	221.1206	P	N-[(3R,4R,5S,6R)-2,4,5-trihydroxy-6-(hydroxymethyl)oxan-3-yl]acetamide	0.8 ± 0.13	1.2 ± 0.31##	0.97 ± 0.21*	1.05
31	321.38	218.0418	P	Alanyl-Glutamine	1.66 ± 0.28	1.22 ± 0.17##	1.74 ± 0.28**	1.35
32	93.14	790.5752	P	PC(P-18:1 (11Z)/20:5 (5Z,8Z,11Z,14Z,17Z))	5.53 ± 1.7	3.54 ± 0.78##	6.48 ± 1.92**	1.29
33	216.41	112.0505	P	Cytosine	7.16 ± 0.74	4.83 ± 1.47##	7.02 ± 0.34**	1.49
34	394.61	217.0658	P	N-a-Acetyl-L-arginine	0.11 ± 0.06	0.19 ± 0.02##	0.12 ± 0.03**	1.29
35	434.06	294.1542	P	Glutaminylphenylalanine	6.9 ± 1.3	4.89 ± 1.58##	6.57 ± 1.57*	1.08
36	417.04	261.1436	P	gamma-Glutamylleucine	9.44 ± 2.92	6.57 ± 1.56##	8.71 ± 2.98*	1.15
37	407.92	142.0859	P	L-Hypoglycin A	1.99 ± 0.26	4.81 ± 1.74##	3.48 ± 0.49*	1.02
38	309.92	341.8941	P	Dihydro-O-methylsterigmatocystin	0.56 ± 0.21	1.01 ± 0.25##	0.72 ± 0.2**	1.47
39	496.99	240.1098	P	6-Lactoyltetrahydropterin	0.65 ± 0.1	1.49 ± 0.53##	1.07 ± 0.53*	1.11
40	213.38	194.0358	P	Phosphocreatinine	0.35 ± 0.15	0.94 ± 0.19##	0.62 ± 0.23*	1.17

Compared to control group, #p < 0.05, ##p < 0.01; Compared to model group, *p < 0.05, **p < 0.01; N: negative mode, P: positive mode.

significantly downregulated in the AD model group. After treatment, these metabolites were restored to varying degrees in the HLJDD group.

Additionally, clustering heatmaps were used to show an intuitive visualization of the difference and clustering degree of metabolites among the three groups. Heatmaps of 40 metabolites were constructed and visualized using MetaboAnalyst software. As shown in **Figure 7**, the metabolites in the AD model group, normal control group, and HLJDD group achieved distinct clusters.

Metabolic Pathway Analysis

Metabolic pathway analysis was performed with MetPA using the identified biomarkers as input, which revealed 21 metabolic pathways that may be involved in the dysregulation of metabolism in AD (**Figure 8**). Pathways with impact values over 0.1 were considered as candidate target pathways. Among them, four pathways, namely, histidine metabolism, arginine biosynthesis, pyrimidine metabolism, and alanine, aspartic acid, and glutamate metabolism, have been suggested to be subject to

FIGURE 7 | Hierarchical clustering results of 40 metabolites in ESI+ **(A)** and ESI– **(B)** mode. Note: The standard concentration was the abscissa, with the metabolites name regarded as the ordinate. Each lattice represents a concentration in corresponding sample. The color ranges from blue to red and the shades of color represent different concentration magnitudes. #$p < 0.05$, ##$p < 0.01$ vs. normal group; *$p < 0.05$, **$p < 0.01$ vs. AD model group.

FIGURE 8 | Pathway analysis of 40 potential biomarkers with MetPA. 1. Nitrogen metabolism, 2. Biosynthesis of unsaturated fatty acids, 3. Caffeine metabolism, 4. Aminoacyl-tRNA biosynthesis, 5. Butanoate metabolism, 6. Pantothenate and CoA biosynthesis, 7. Selenocompound metabolism, 8. Folate biosynthesis, 9. Glyoxylate and dicarboxylate metabolism, 10. Glutathione metabolism, 11. Glycerophospholipid metabolism, 12. Tryptophan metabolism, 13. Amino sugar and nucleotide sugar metabolism, 14. beta-Alanine metabolism, 15. Porphyrin and chlorophyll metabolism, 16. Arginine and proline metabolism, 17. Arginine biosynthesis, 18. Histidine metabolism, 19. Pyrimidine metabolism, 20. Alanine, aspartate and glutamate metabolism, 21. D-Glutamine and D-glutamate metabolism.

perturbation by HLJDD to improve the endogenous metabolism of AD.

Targeted Metabolomics
Selection of Metabolites for Targeted Metabolomics and Construction of a Standard Curves

For the screening diagnostic biomarkers, pearson's correlation analysis was used for the correlation analysis of 17 physiological and biochemical indices (skin lesion score, IL-13, IL-17, IL-3, IL-31, IL-33, IL-4, IL-5, TSLP, histamine, HRH4 mRNA, IL-4Rα mRNA, JAK1 mRNA, IgE, IL-4Rα, JAK1, p-JAK1, and HRH4) and 40 potential biomarkers. First, in the normal control group and AD model group, a total of 190 metabolites were significantly associated with physiological and biochemical indices (**Supplementary Figure S11**), which could act as diagnostic biomarkers for AD. Second, in the AD model group and HLJDD group, a total of 190 metabolites were significantly associated with macroscopic indexes (**Supplementary Figure S12**), which could act as a potential biomarker for AD treated with HLJDD. To increase the diagnostic capability of the

potential biomarkers, we took the intersection of the two sets of predictions. Finally, 23 metabolites (prostaglandin D1, phosphocreatinine, n-methyl-d-aspartic acid, n-hydroxymethylnorcotinine, malic acid, lysopc (24:1 (15z)), linolelaidic acid, l-alloisoleucine, l-alanine, humulinone, glutaric acid, gamma-linolenic acid, dihydro-o-methylsterigmatocystin, deoxyuridine, d-phenyllactic acid, carnosine, biliverdin, alanyl-glutamine, 4-imidazolone-5-propionic acid, 3,7-dimethylpurine-2,6-dione, 2-hydroxy-2-methylbutanedioic acid, 1h-pyrimidine-2,4-dione, and (z)-tetracos-15-enoic acid) were selected as diagnostic biomarkers of AD. Considering the accuracy of metabolites and the diversity detected in each sample, 14 endogenous metabolites (DL-malic acid, glutaric acid, N-methyl-D-aspartic acid, linolelaidic acid, gamma-linolenic acid, L-alloisoleucine, L-carnosine, phosphocreatinine, L-alanine, 2′-deoxyuridine, prostaglandin D1, 1H-pyrimidine-2,4-dione, L-alanyl-L-glutamine, and biliverdine) were selected for targeted metabolomics analysis. As shown in **Figure 9**, a standard curve of 14 endogenous metabolites was established. The

FIGURE 9 | Standard curves of 14 different metabolites of DL-Malic acid, Glutaric acid, N-Methyl-D-aspartic acid, linolelaidic acid, γ-Linolenic acid, L-Alloisoleucine, L-Carnosine, phosphocreatinine, L-Alanine, 2′-Deoxyuridine, Prostaglandin D1, 1H-pyrimidine-2,4-dione, L-Alanyl-L-Glutamine, and Biliverdine.
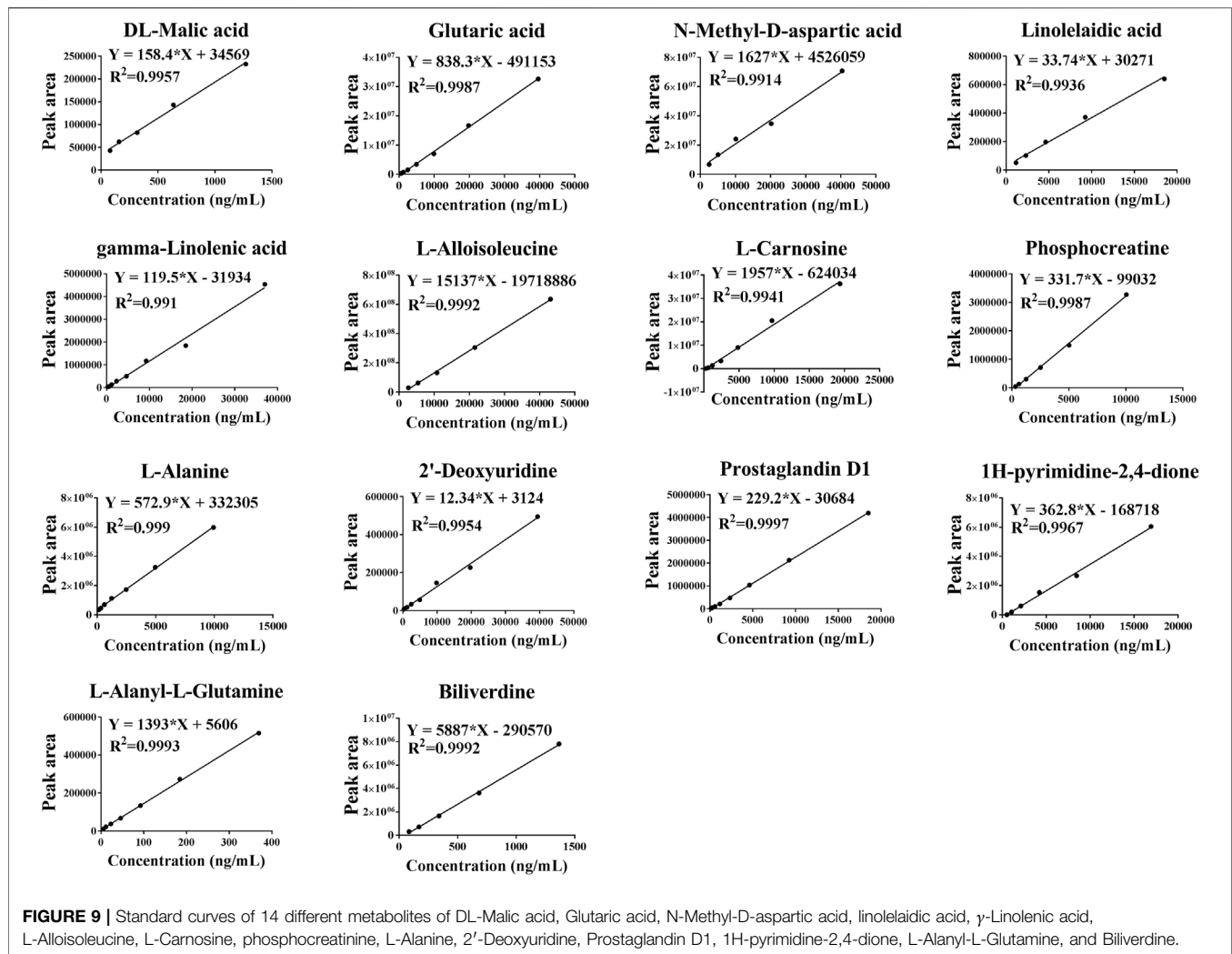
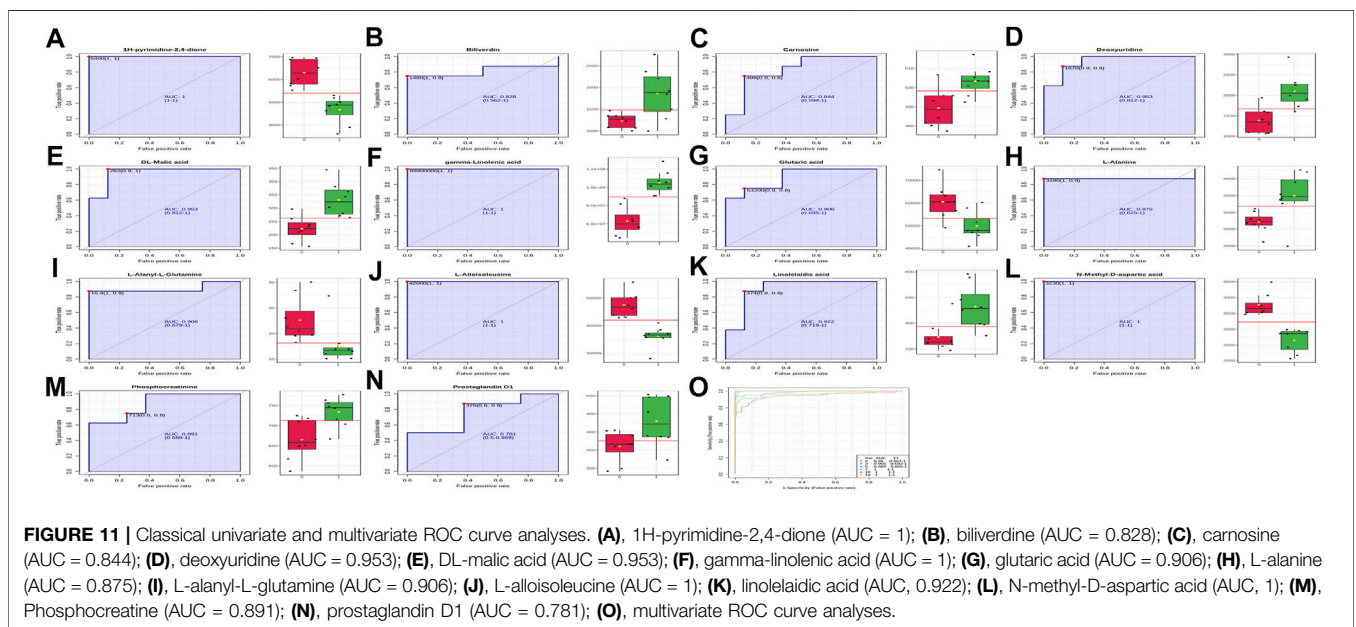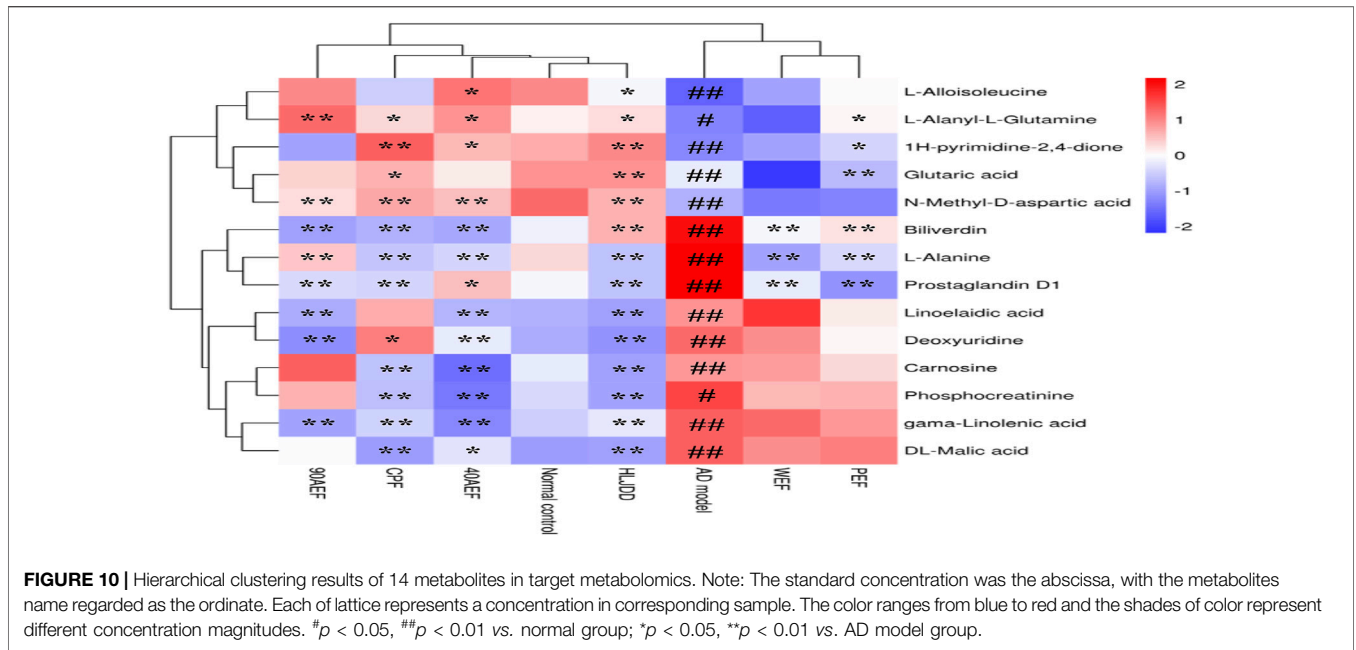curve fit all values of R^2 > 0.9, indicating that the concentration calculation based on these curves was accurate.

Assessment of 14 Metabolites in HLJDD and its Fractions by Targeted Metabolomics

As shown in **Figure 10**, compared with the normal control group, L-alloisoleucine, L-alanyl-L-glutamine, glutaric acid, 1H-pyrimidine-2,4-dione, and N-methyl-D-aspartic acid were significantly downregulated, and glutaric acid, N-methyl-D-aspartic acid, linolelaidic acid, gamma-linolenic acid, L-carnosine, phosphocreatinine, L-alanine, 2′-deoxyuridine, prostaglandin D1, L-alanyl-L-glutamine, biliverdine, and DL-malic acid were significantly upregulated in the AD model group. After treatment, these metabolites were restored to varying degrees in the HLJDD group, which was also consistent with the findings of the untargeted metabolomics analysis. Meanwhile, we found that these metabolites were also restored to varying degrees in the CPF, 40AEF, 90AEF, WEF, and PEF groups, indicating that CPF, 40AEF, 90AEF, WEF, and PEF exhibited different degrees of therapeutic activity against AD, especially HLJDD, 40AEF, and CPF. Hierarchical clustering

analysis was performed using MetaboAnalyst software, the results of which revealed that there were two clusters (AD model group, WEF, PEF; normal control group, HLJDD, CPF, 40AEF, 90AEF), which further validated the therapeutic effects of HLJDD and its fractions, especially HLJDD, 40AEF, and CPF. Therefore, 40AEF and CPF are considered the most important components of HLJDD for ameliorating AD.

Evaluation of Diagnostic Efficacy of Potential Biomarkers

ROC curves were used to assess the sensitivity and specificity of the diagnostic performance of potential biomarkers (Hao et al., 2010; Li, et al., 2014a). Diagnostic accuracy was analyzed by area under curve (AUC) of ROC, and AUC was considered to be of good accuracy when AUC > 0.7 (Abdel-Gawad et al., 2009). Classical univariate ROC curve analyses and multivariate ROC curve based exploratory analysis (Explorer) were performed using MetaboAnalyst 5.0 (https://www.metaboanalyst.ca/). The results of classical univariate ROC curve analyses indicated that the AUC of 14 metabolites was greater than 0.7 (**Figures 11A–N**). The results of the multivariate ROC curve based exploratory analysis
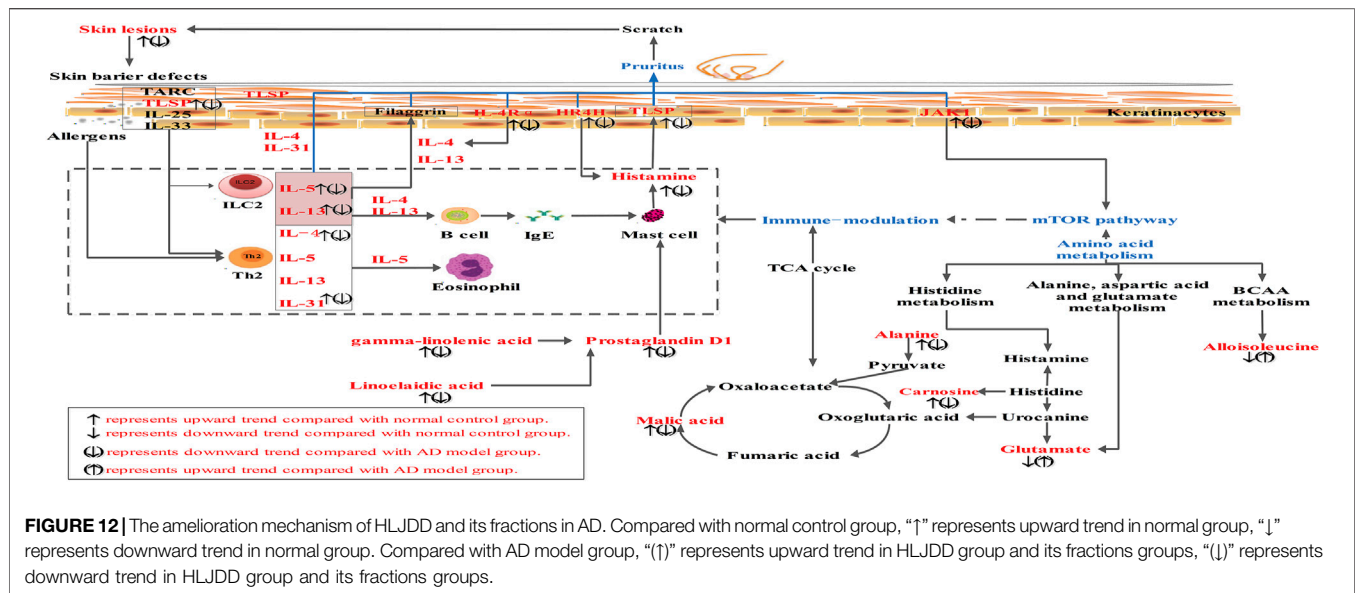
FIGURE 10 | Hierarchical clustering results of 14 metabolites in target metabolomics. Note: The standard concentration was the abscissa, with the metabolites name regarded as the ordinate. Each of lattice represents a concentration in corresponding sample. The color ranges from blue to red and the shades of color represent different concentration magnitudes. $^{\#}p < 0.05$, $^{\#\#}p < 0.01$ vs. normal group; $^{*}p < 0.05$, $^{**}p < 0.01$ vs. AD model group.

FIGURE 11 | Classical univariate and multivariate ROC curve analyses. **(A)**, 1H-pyrimidine-2,4-dione (AUC = 1); **(B)**, biliverdine (AUC = 0.828); **(C)**, carnosine (AUC = 0.844); **(D)**, deoxyuridine (AUC = 0.953); **(E)**, DL-malic acid (AUC = 0.953); **(F)**, gamma-linolenic acid (AUC = 1); **(G)**, glutaric acid (AUC = 0.906); **(H)**, L-alanine (AUC = 0.875); **(I)**, L-alanyl-L-glutamine (AUC = 0.906); **(J)**, L-alloisoleucine (AUC = 1); **(K)**, linolelaidic acid (AUC, 0.922); **(L)**, N-methyl-D-aspartic acid (AUC, 1); **(M)**, Phosphocreatine (AUC = 0.891); **(N)**, prostaglandin D1 (AUC = 0.781); **(O)**, multivariate ROC curve analyses.

indicated that the AUC was greater than 0.9 (**Figure 11O**). Therefore, these metabolites may be potential candidate biomarkers for predicting AD.

DISCUSSION

HLJDD is a traditional Chinese medicine composed of four herbs, *Coptis chinensis* Franch., *Scutellaria baicalensis* Georgi, *Phellodendron amurense* Rupr., and *Gardenia jasminoides* J. Ellis. It is frequently prescribed due to its

effectiveness against serious illness, including those of the skin (Chen et al., 2017; Chen et al., 2016). With these properties, HLJDD has a curative effect in the treatment of AD (Qi et al., 2019). Clinical and experimental studies have confirmed that HLJDD is an effective drug for the treatment of AD. However, the effective ingredients and underlying molecular mechanisms have not yet been fully explored (Kobayashi et al., 2004). Previous studies have shown that the major constituents of HLJDD include alkaloids, flavonoids, iridoids, organic acids, and amino acids (Wang et al., 2020). Therefore, further research is needed to elucidate

FIGURE 12 | The amelioration mechanism of HLJDD and its fractions in AD. Compared with normal control group, "↑" represents upward trend in normal group, "↓" represents downward trend in normal group. Compared with AD model group, "(↑)" represents upward trend in HLJDD group and its fractions groups, "(↓)" represents downward trend in HLJDD group and its fractions groups.

the possible active ingredients responsible for the anti-AD action of HLJDD.

Traditional Chinese medicine always exhibits "multi-component" and "multi-target" characteristics in the treatment of diseases, which is a big challenge to clarify the pharmacodynamic components of Chinese drugs. In general, decoctions or alcoholic extracts of Chinese drugs were split into multiple fractions, which were used to clarify its substance basis (Li et al., 2014a). Based on previous laboratory research (Chen et al., 2021; Han et al., 2020), we developed a reliable method for the rapid screening of chemical constituents and the evaluation of non-similarity degrees of splitting fractions of HLJDD using HPLC and UPLC-Q-TOF/MS/MS techniques. In this study, HLJDD was split into five fractions, and a total of 72 chemical constituents were analyzed and identified, where the different fractions showed significant chemical differences (>81%). The main components of 40AEF, 90AEF, PEF, and WEF were alkaloids, flavonoids, and a few alkaloids, iridoids, organic acids, and amino acids, respectively, which provides insights into understanding the complex compounds of HLJDD and further analyzing the pharmacological studies of different fractions.

Furthermore, a DNFB-induced AD mouse model was used to explore the therapeutic effects of HLJDD and its fractions on AD. Owing to its simplicity and ease of use, high repeatability, and easy quantization of clinical scores, the model has been widely used for anti-AD drug discovery and development (Shiohara et al., 2004; Xiong et al., 2020; Zeng et al., 2021). Our results showed that typical allergic responses, including itching, increased ear and epidermal thickness, swelling, dryness, and erythema were observed in the AD model, which was consistent with a previous study (Xiong et al., 2020). However, the above symptoms in the dorsal skin of mice in the HLJDD group and the groups treated with its fractions were remarkably improved. The results indicated that HLJDD and its fractions had therapeutic effects on AD, especially 40AEF and CPF. Furthermore,

combined with the results of physiological and biochemical indices and metabolomics, the amelioration mechanism of HLJDD in AD was proposed, as shown in **Figure 12**.

Pruritus is a major clinical feature of AD, and AD is considered a prototype of chronic pruritic dermatosis (Ständer and Steinhoff, 2010). The pathogenesis of AD mainly occurs as a result of immune system disorders and epidermal barrier dysfunction, which may be related to genetic, immune, and environmental changes (Ständer and Steinhoff, 2010). Skin barrier damage and immunological dysfunction are key pathogenic components of AD. Th2 cells secrete cytokines, such as IL-4, IL-5, and IL-13, which are important for AD development, especially in the acute phase of AD. Skin barrier damage induces the release of large amounts of keratinocyte-derived proinflammatory cytokines, such as IL-33 and TSLP, from keratinocytes. It also activates the inflammatory cascade, mainly involving Th2 cytokines, such as IL-4, IL-13, and IL-5 (Weidinger et al., 2018). The results of our study indicated that the levels of IL-33, TSLP, IL-4, IL-13, and IL-5 were significantly upregulated in the AD model group, and that HLJDD and its fractions could reverse these effects. Histamine is the first and most well-known pruritogen (Simons and Simons, 2011). Itching sensation can be transmitted by the histamine pathway. In our study, the levels of histamine and IL-31 were significantly upregulated in the AD model group, and higher levels of IL-4Rα, JAK1, and HRH4 expression were detected in the AD model group by PCR and WB analysis. HLJDD and its fractions could also reverse these effects. Previous studies have indicated that IL-31, IL-4Rα, JAK1, and HRH4 are strongly associated with pruritus in AD (Oetjen et al., 2017). Therefore, HLJDD exhibited anti-AD effects by regulating IL-4Rα, JAK1, HRH4, histamine, and relative cytokines (IL-33, TSLP, IL-4, IL-13, and IL-5). 40AEF and CPF had much greater therapeutic action, which was considered the most important component of HLJDD for ameliorating AD.

Diseases often impair the normal metabolism of the body, and disordered metabolic conditions can be effectively measured by metabolomics studies, aiding in the diagnosis and treatment of diseases (Yu et al., 2021). Therefore, in the current study, we propose to use the untargeted and targeted metabolomics method to systematically explore the therapeutic mechanism of HLJDD and its fractions in the treatment of AD, which will allow us to specifically understand how the signaling has been altered during the treatment, and how changes in signaling can attenuate metabolic disorders in the body. Forty significant biomarkers were identified and selected using untargeted metabolomics. Metabolic pathway analysis indicated that these differential metabolites may be involved in histidine metabolism, arginine biosynthesis, pyrimidine metabolism, and alanine, aspartic acid, and glutamate metabolism, have been suggested to be subject to perturbation by HLJDD to improve the endogenous metabolism of AD. Further, for screening diagnostic biomarkers, Pearson's correlation analysis was used for the correlation analysis of 17 physiological and biochemical indices and 40 potential biomarker data. Fourteen endogenous metabolites (DL-malic acid, glutaric acid, N-methyl-D-aspartic acid, linolelaidic acid, gamma-linolenic acid, L-alloisoleucine, L-carnosine, phosphocreatinine, L-alanine, 2′-deoxyuridine, prostaglandin D1, 1H-pyrimidine-2,4-dione, L-alanyl-L-glutamine, and biliverdine) were selected for targeted metabolomic analysis. The results of targeted metabolomics analysis indicated that these metabolites were restored to varying degrees in the HLJDD group, which was also consistent with the findings of untargeted metabolomics analysis. Meanwhile, we found that these metabolites were also restored to varying degrees in the CPF, 40AEF, 90AEF, WEF, and PEF groups, especially HLJDD, 40AEF, and CPF. Interestingly, 40AEF and CPF had much greater therapeutic action, which further validated that 40AEF and CPF were the most important components of HLJDD for ameliorating AD. In addition, the results of univariate and multivariate ROC curve-based exploratory analysis indicated that these metabolites may be potential candidate biomarkers for predicting AD.

Among these differential metabolites, fatty acids, including gamma-linolenic acid and linolelaidic acid, were increased in the AD model group. Fatty acids have been considered to play a critical role in inflammatory responses because they are a source of various lipid mediators (Sala-Vila et al., 2010; Schafer and Kragballe, 1991; Trak-Fellermeier et al., 2004). Gamma-linolenic acid has been reported to reduce skin water loss and promote skin epidermal cell proliferation. In patients with dry skin and moderate AD, long-term diet treatment with high gamma-linolenic acid has been found to gradually restore skin barrier function, reduce water loss in the skin, and decrease inflammatory factor expression in AD patients (Kawamura et al., 2011). Previous studies have revealed that prostaglandin D1 upregulation is involved in the prevention of AD by suppressing both mast cell and keratinocyte activation, which is one mechanism by which dihomo-g-linolenic acid prevents the development of atopic dermatitis (Amagai et al., 2015). Interestingly, higher levels of gamma-linolenic acid, linolelaidic acid, and prostaglandin D1 in the AD model group were observed in our study. After

treatment, the levels of gamma-linolenic acid, linolelaidic acid, and prostaglandin D1 were downregulated in HLJDD and its fractions. Therefore, in the event of AD, there was a need for more gamma-linolenic acid, linolelaidic acid, and prostaglandin D1 in order to combat mast cell and keratinocyte activation. After treatment, higher levels of metabolites were also improved over time following the symptoms of AD amelioration. Thus, HLJDD may play an anti-inflammatory role during the treatment of AD by downregulating the expression of gamma-linolenic acid. The levels of amino acids, including L-alloisoleucine, N-methyl-D-aspartic acid, and L-alanyl-L-glutamine, were decreased and L-alanine was increased in the AD model group. Specifically, isoleucine is a branched-chain amino acid (BCAA). Changes in the metabolites involved in the BCAA pathway are known to influence the regulation of mTOR (Jewell and Guan, 2013; Zhenyukh et al., 2017), which plays a vital role in epidermal barrier formation and the signaling axis for the control of filaggrin as the fundamental pathophysiology of AD (Xda et al., 2020; Yang et al., 2014). Both N-methyl-D-aspartate and L-alanyl-L-glutamine are important excitatory neurotransmitters in the central nervous system and are associated with scratching and pathological modification behavior in AD-like mice (Fujii et al., 2018; Funakushi et al., 2011). The etiology of AD has been linked to deficiencies in the histamine-rich epidermal barrier protein filaggrin (Palmer et al., 2006). Carnosine and histamine are involved in histidine metabolism; their levels were significantly upregulated in the AD model group, demonstrating that histidine metabolism disorders occurred in AD. Similarly, the levels of these amino acids were reversed in the HLJDD and its fraction groups. The tricarboxylic acid (TCA) cycle, reflected in the altered DL-malic acid level found in this study, can shape immune cell responses via changes in the metabolic pathways of immune cells (O'Neill et al., 2016). In addition, the other differential metabolites (phosphocreatinine, 2′-deoxyuridine, 1H-pyrimidine-2,4-dione, and biliverdine) identified in this study also have implications for AD treatment.

CONCLUSION

The present study utilized chemistry, biochemistry, and metabolomics analysis to dissect the pharmacological mechanism and substance basis of HLJDD in AD. This paper is the first to report on the development and validation of a multivariate analysis method to qualitatively and quantitatively analyze the non-similarity degree, which was suited to the non-similarity degrees of splitting fractions of HLJDD. Further, HLJDD exhibited anti-AD effects by inhibiting itching and enhancing immunity, which in turn regulating the levels of relative metabolites, and CPF and 40AEF were considered the most important components of HLJDD. This study provided novel insight into how chemistry, biochemistry, and metabolomics could be used as effective tools for elucidating the efficacy of HLJDD on AD.

DATA AVAILABILITY STATEMENT

The original contributions presented in the study are included in the article/**Supplementary Material**, further inquiries can be directed to the corresponding author.

ETHICS STATEMENT

The animal study was reviewed and approved by the Bioethics Committee of Shanghai Tenth People's Hospital (ID no. SHDSYY-2020-9001).

AUTHOR CONTRIBUTIONS

JC and YX performed the experiments, analyzed the data, and wrote the article. JC and JC provided help with the animal experiments. SC, BS, and ZJ provided help with the data analysis. JC and YX designed the study. JC, SC, and YX modified the final article.

SUPPLEMENTARY MATERIAL

The Supplementary Material for this article can be found online at: https://www.frontiersin.org/articles/10.3389/fphar.2021.770524/full#supplementary-material

REFERENCES

Abdel-Gawad, T. A., El-Hodhod, M. A., Ibrahim, H. M., and Michael, Y. W. (2009). Gastroesophageal Reflux in Mechanically Ventilated Pediatric Patients and its Relation to Ventilator-Associated Pneumonia. *Crit. Care* 13 (Suppl. 1), R164. doi:10.1186/cc8134

Amagai, Y., Oida, K., Matsuda, A., Jung, K., Kakutani, S., and Tanaka, T. (2015). Dihomo-γ-linolenic Acid Prevents the Development of Atopic Dermatitis through Prostaglandin D1 Production in NC/Tnd Mice. *J. Dermatol. Sci.* 79 (1), 30–37. doi:10.1016/j.jdermsci.2015.03.010

Blume-Peytavi, U., Bagot, M., Tennstedt, D., Saint Aroman, M., Stockfleth, E., Zlotogorski, A., et al. (2019). Dermatology Today and Tomorrow: from Symptom Control to Targeted Therapy. *J. Eur. Acad. Dermatol. Venereol.* 33 Suppl, 3–36. doi:10.1111/jdv.15335

Bonamonte, D., Filoni, A., Vestita, M., Romita, P., Foti, C., and Angelini, G. (2019). The Role of the Environmental Risk Factors in the Pathogenesis and Clinical Outcome of Atopic Dermatitis. *Biomed. Res. Int.* 2019 (2), 1–11. doi:10.1155/2019/2450605

Cao, W., Wang, X., Li, H., Shi, X., Fan, W., Zhao, S., et al. (2015). Studies on Metabolism of Total Glucosides of Paeony from Paeoniae Radix Alba in Rats by UPLC-Q-TOF-MS/MS. *Biomed. Chromatogr. : BMC.* 29 (11), 1769–1779. doi:10.1002/bmc.3493

Chen, G., Xu, Y., Jing, J., Mackie, B., Zheng, X., Zhang, X., et al. (2017). The Anti-sepsis Activity of the Components of Huanglian Jiedu Decoction with High Lipid A-Binding Affinity. *Int. immunopharmacology* 46, 87–96. doi:10.1016/j.intimp.2017.02.025

Chen, J., Dou, P., Xiao, H., Dou, D., Han, X., and Kuang, H. (2021). Application of Proteomics and Metabonomics to Reveal the Molecular Basis of Atractylodis Macrocephalae Rhizome for Ameliorating Hypothyroidism Instead of Hyperthyroidism. *Front. Pharmacol.* 12. doi:10.3389/fphar.2021.664319

Chen, Q., Wang, F., Cai, Y., Zhang, Y., Fang, J., Qi, L., et al. (2020a). Untargeted Metabolomics and Lipidomics Uncovering the Cardioprotective Effects of Huanglian Jiedu Decoction on Pathological Cardiac Hypertrophy and Remodeling. *J. ethnopharmacology* 270, 113646. doi:10.1016/j.jep.2020.113646

Chen, Y., Xian, Y., Lai, Z., Loo, S., Chan, W. Y., Lin, Z., et al. (2016). Anti-inflammatory and Anti-allergic Effects and Underlying Mechanisms of Huang-Lian-Jie-Du Extract: Implication for Atopic Dermatitis Treatment. *J. ethnopharmacology* 185, 41–52. doi:10.1016/j.jep.2016.03.028

Chen, Y., Xian, Y., Loo, S., Lai, Z., Chan, W. Y., Liu, L., et al. (2020b). Huang-Lian-Jie-Du Extract Ameliorates Atopic Dermatitis-like Skin Lesions Induced by 2,4-dinitrobenzene in Mice via Suppression of MAPKs and NF-Kb Pathways. *J. ethnopharmacology* 249, 112367. doi:10.1016/j.jep.2019.112367

Choi, H., Kim, D., Nam, S., Lim, S., Hwang, J.- S., Park, K. S., et al. (2018). Manifestation of Atopic Dermatitis-like Skin in TNCB-Induced NC/Nga Mice Is Ameliorated by Topical Treatment of Substance P, Possibly through Blockade of Allergic Inflammation. *Exp. Dermatol.* 27 (4), 396–402. doi:10.1111/exd.13421

Daya, M., and Barnes, K. C. (2019). African American Ancestry Contribution to Asthma and Atopic Dermatitis. *Ann. Allergy Asthma Immunol.* 122 (5), 456–462. doi:10.1016/j.anai.2019.02.009

Eckert, L., Gupta, S., Gadkari, A., Mahajan, P., and Gelfand, J. M. (2019). Burden of Illness in Adults with Atopic Dermatitis: Analysis of National Health and Wellness Survey Data from France, Germany, Italy, Spain, and the United Kingdom. *J. Am. Acad. Dermatol.* 81 (1), 187–195. doi:10.1016/j.jaad.2019.03.037

Ferreres, F., Llorach, R., and Gil-Izquierdo, A. (2004). Characterization of the Interglycosidic Linkage in Di-, Tri-, Tetra- and Pentaglycosylated Flavonoids and Differentiation of Positional Isomers by Liquid Chromatography/electrospray Ionization Tandem Mass Spectrometry. *J. Mass Spectrom.* 39 (3), 312–321. doi:10.1002/jms.586

Fujii, M., Takeuchi, K., Umehara, Y., Takeuchi, M., Nakayama, T., Ohgami, S., et al. (2018). Barbiturates Enhance Itch-Associated Scratching in Atopic Dermatitis Mice: A Possible Clue to Understanding Nocturnal Pruritus in Atopic Dermatitis. *Eur. J. Pharmacol.* 836, 57–66. doi:10.1016/j.ejphar.2018.08.018

Funakushi, N., Yamaguchi, T., Jiang, J., Imamura, S., Kuhara, T., Suto, H., et al. (2011). Ameliorating Effect of Yokukansan on the Development of Atopic Dermatitis-like Lesions and Scratching Behavior in Socially Isolated NC/Nga Mice. *Arch. Dermatol. Res.* 303 (9), 659–667. doi:10.1007/s00403-011-1137-9

Guo, M., Zhao, B., Liu, H., Zhang, L., Peng, L., Qin, L., et al. (2014). A Metabolomic Strategy to Screen the Prototype Components and Metabolites of Shuang-Huang-Lian Injection in Human Serum by Ultra Performance Liquid Chromatography Coupled with Quadrupole Time-Of-Flight Mass Spectrometry. *J. Anal. Methods Chem.* 2014, 241505. doi:10.1155/2014/241505

Han, X., Xiao, H., Chen, J., Xu, W., and Dou, D. (2020). The Substance Basis of Poria Ameliorates Hypothyroidism Other Than Hyperthyroidism Based on Proteomics and Metabolomics. *FASEB J.* 34 (9), 11970–11982. doi:10.1096/fj.202000984R

Hao, W., Xue, R., Tang, Z., Deng, C., Liu, T., Zeng, H., et al. (2010). Metabolomic Investigation of Gastric Cancer Tissue Using Gas Chromatography/mass Spectrometry. *Anal. Bioanal. Chem.* 396 (4), 1385–1395. doi:10.1007/s00216-009-3317-4

Hung, J. Y., Yang, C. J., Tsai, Y. M., Huang, H. W., and Huang, M. S. (2010). Antiproliferative Activity of Aucubin Is through Cell Cycle Arrest and Apoptosis in Human Non-small Cell Lung Cancer A549 Cells. *Clin. Exp. Pharmacol. Physiol.* 35 (9), 995–1001. doi:10.1111/j.1440-1681.2008.04935.x

Jewell, J. L., and Guan, K. L. (2013). Nutrient Signaling to mTOR and Cell Growth. *Trends Biochem. Sci.* 38 (5). doi:10.1016/j.tibs.2013.01.004

Kawamura, A., Ooyama, K., Kojima, K., Kachi, H., Abe, T., Amano, K., et al. (2011). Dietary Supplementation of Gamma-Linolenic Acid Improves Skin Parameters in Subjects with Dry Skin and Mild Atopic Dermatitis. *J. oleo Sci.* 60 (12), 597–607. doi:10.5650/jos.60.597

Kim, B. K., Kim, J. Y., Kang, M. K., Yang, M. S., Park, H. W., Min, K. U., et al. (2016). Allergies Are Still on the Rise? A 6-year Nationwide Population-Based Study in Korea. *Allergol. Int. official J. Jpn. Soc. Allergol.* 65 (2), 186–191. doi:10.1016/j.alit.2015.11.002

Kobayashi, H., Takahashi, K., Mizuno, N., Kutsuna, H., and Ishii, M. (2004). An Alternative Approach to Atopic Dermatitis: Part I-Case-Series Presentation. *Evid Based. Complement. Altern. Med. : eCAM* 1 (1), 49–62. doi:10.1093/ecam/neh015

Koo, H. J., Song, Y. S., Kim, H. J., Lee, Y. H., Hong, S. M., Kim, S. J., et al. (2004). Antiinflammatory Effects of Genipin, an Active Principle of Gardenia. *Eur. J. Pharmacol.* 495 (2-3), 201–208. doi:10.1016/j.ejphar.2004.05.031

Krzymińska, A., Gsecka, M., and Magdziak, Z. (2020). Molecules Content of Phenolic Compounds and Organic Acids in the Flowers of Selected Tulipa Gesneriana Cultivars. *Molecules* 25, 5627. doi:10.3390/molecules25235627

Lam, W. K. (2010). Activation of Human Eosinophils and Epidermal Keratinocytes by Th2 Cytokine IL-31: Implication for the Immunopathogenesis of Atopic Dermatitis. *Int. Immunol.* 22 (6), 453. doi:10.1093/intimm/dxq027

Li, K., Cao, Y., Jiao, S., Du, G. H., Du, Y. G., Qin, X. M., et al. (2020). Structural Characterization and Immune Activity Screening of Polysaccharides with Different Molecular Weights from Astragali Radix. *Front. Pharmacol.* 11, 582091. doi:10.3389/fphar.2020.582091

Li, L., Ran, X., Xu, Y., Bin, L., and De-Qiang, D. (2014a). A Method for Evaluation of Non-similarity Degrees between Splitting Fractions of Atractylodis Macrocephalae Rhizoma. *Chin. J. Anal. Chem.* 42 (03), 343–348. doi:10.3724/SP.J.1096.2014.30981

Li, Y., Song, X., Zhao, X., Zou, L., and Xu, G. (2014b). Serum Metabolic Profiling Study of Lung Cancer Using Ultra High Performance Liquid Chromatography/quadrupole Time-Of-Flight Mass Spectrometry. *J. Chromatogr. B, Anal. Tech. Biomed. Life Sci.* 966, 147–153. doi:10.1016/j.jchromb.2014.04.047

Ma, H., Liu, Y., Mai, X., Liao, Y., Zhang, K., Liu, B., et al. (2016). Identification of the Constituents and Metabolites in Rat Plasma after Oral Administration of HuanglianShangqing Pills by Ultra High-Performance Liquid Chromatography/quadrupole Time-Of-Flight Mass Spectrometry. *J. Pharm. Biomed. Anal.* 125, 194–204. doi:10.1016/j.jpba.2016.03.038

Maimaiti, Z., Turak, A., Ma, Q., Liu, G., and Aisa, H. A. (2020). Quantitative Determination of Marker Compounds and Fingerprint Analysis of the Seeds of Vernonia Anthelmintica. *Int. J. Anal. Chem.* 11, 8859425. doi:10.1155/2020/8859425

O'Neill, L. A. J., Kishton, R. J., and Rathmell, J. (2016). A Guide to Immunometabolism for Immunologists. *Nat. Rev. Immunol.* 16, 553–565. doi:10.1038/nri.2016.70

Oetjen, L. K., Mack, M. R., Feng, J., Whelan, T. M., Niu, H., Guo, C. J., et al. (2017). Sensory Neurons Co-opt Classical Immune Signaling Pathways to Mediate Chronic Itch. *Cell* 171, 217–228. doi:10.1016/j.cell.2017.08.006

Olsson, M., Bajpai, R., Wee, L. W. Y., Yew, Y. W., Koh, M. J. A., Thng, S., et al. (2020). The Cost of Childhood Atopic Dermatitis in a Multi-ethnic Asian Population: a Cost-of-illness Study. *Br. J. Dermatol.* 182 (5), 1245–1252. doi:10.1111/bjd.18442

Otsuka, A., Honda, T., Doi, H., Miyachi, Y., and Kabashima, K. (2011). An H1-Histamine Receptor Antagonist Decreases Serum Interleukin-31 Levels in Patients with Atopic Dermatitis. *Br. J. Dermatol.* 164 (2), 455–456. doi:10.1111/j.1365-2133.2010.10083.x

Palmer, C., Irvine, A. D., Terron-Kwiatkowski, A., Zhao, Y., Liao, H., Lee, S. P., et al. (2006). Common Loss-Of-Function Variants of the Epidermal Barrier Protein Filaggrin Are a Major Predisposing Factor for Atopic Dermatitis. *Nat. Genet.* 38 (4), 441–446. doi:10.1038/ng1767

Pico-Hernández, S. M., Murillo-Méndez, C. J., and López-Giraldo, L. J. (2020). Extraction, Separation, and Evaluation of Antioxidant Effect of the Different Fractions of Polyphenols from cocoa beans. *Revista Colombiana de Quimica* 49 (3), 19–27. doi:10.15446/rcq.v49n3.84082

Qi, Y., Zhang, Q., and Zhu, H. (2019). Huang-Lian Jie-Du Decoction: a Review on Phytochemical, Pharmacological and Pharmacokinetic Investigations. *Chin. Med.* 14, 57. doi:10.1186/s13020-019-0277-2

Raap, U., Werfel, T., Goltz, C., Deneka, N., Langer, K., Bruder, M., et al. (2006). Circulating Levels of Brain ϒerived Neurotrophic Factor Correlate with Disease Severity in the Intrinsic Type of Atopic Dermatitis. *Allergy* 61 (12), 1416–1418. doi:10.1111/j.1398-9995.2006.01210.x

Rasouli, H., Hosseini-Ghazvini, M. B., and Khodarahmi, R. (2019). Therapeutic Potentials of the Most Studied Flavonoids: Highlighting Antibacterial and Antidiabetic Functionalities - ScienceDirect. *Stud. Nat. Prod. Chem.* 60, 85–122. doi:10.1016/b978-0-444-64181-6.00003-6

Sala-Vila, A., Miles, E. A., and Calder, P. C. (2010). Fatty Acid Composition Abnormalities in Atopic Disease: Evidence Explored and Role in the Disease Process Examined. *Clin. Exp. Allergy J. Br. Soc. Allergy Clin. Immunol.* 38 (9), 1432–1450. doi:10.1111/j.1365-2222.2008.03072.x

Sandhu, J. K., Nicole, S., Nazanin, E.-C., and Armstrong, A. W. (2019). Economic Burden of Cutaneous Infections in Children and Adults with Atopic Dermatitis. *Pediatr. Dermatol.* 36 (3), 303–310. doi:10.1111/pde.13828

Schafer, L., and Kragballe, K. (1991). Abnormalities in Epidermal Lipid Metabolism in Patients with Atopic Dermatitis. *J. Invest. Dermatol.* 96 (1), 10–15. doi:10.1111/1523-1747.ep12514648

Serrano, L., Patel, K., and Silverberg, J. (2019). Association between Atopic Dermatitis and Extracutaneous Bacterial and Mycobacterial Infections: A Systematic Review and Meta-Analysis. *J. Am. Acad. Dermatol.* 80 (4), 904–912. doi:10.1016/j.jaad.2018.11.028

Shiohara, T., Hayakawa, J., and Mizukawa, Y. (2004). Animal Models for Atopic Dermatitis: Are They Relevant to Human Disease? *J. Dermatol. Sci.* 36 (1), 1–9. doi:10.1016/j.jdermsci.2004.02.013

Simons, F., and Simons, K. (2011). Histamine and H1-Antihistamines: Celebrating a century of Progress. *J. Allergy Clin. Immunol.* 128 (6), 1139–1150. e1134. doi:10.1016/j.jaci.2011.09.005

Ständer, S., and Steinhoff, M. (2010). Pathophysiology of Pruritus in Atopic Dermatitis: an Overview. *Exp. Dermatol.* 11 (1), 12–24. doi:10.1034/j.1600-0625.2002.110102.x

Sur, B., Lee, B., Yeom, M., Hong, J. H., Kwon, S., Kim, S. T., et al. (2016). Bee Venom Acupuncture Alleviates Trimellitic Anhydride-Induced Atopic Dermatitis-like Skin Lesions in Mice. *BMC Complement. Altern. Med.* 16 (1), 38. doi:10.1186/s12906-016-1019-y

Trak-Fellermeier, M. A., Brasche, S., Winkler, G., Koletzko, B., and Heinrich, J. (2004). Food and Fatty Acid Intake and Atopic Disease in Adults. *Eur. Respir. J.* 23 (4), 575. doi:10.1183/09031936.04.00074404

Wang, G., Wang, J., and Guan, R. (2020). Novel Phospholipid-Based Labrasol Nanomicelles Loaded Flavonoids for Oral Delivery with Enhanced Penetration and Anti-brain Tumor Efficiency. *Curr. Drug Deliv.* 17 (3), 229–245. doi:10.2174/1567201817666200210120950

Wang, H., Chen, C., Liu, Y., Yanga, X., and Xiao, H. (2015). Metabolic Profile of Yi-Xin-Shu Capsule in Rat by Ultra-performance Liquid Chromatography Coupled with Quadrupole Time-Of-Flight Tandem Mass Spectrometry Analysis. *Rsc Adv.* 5 (98), 80583–80590. doi:10.1039/c5ra14260a

Wang, K. X., Gao, Y., Gong, W. X., Ye, X. F., Fan, L. Y., Wang, C., et al. (2020). A Novel Strategy for Decoding and Validating the Combination Principles of Huanglian Jiedu Decoction from Multi-Scale Perspective. *Front. Pharmacol.* 11, 567088. doi:10.3389/fphar.2020.567088

Wang, L., Xiao, H., Liang, X., and Bi, K. S. (2002). Vectorial Angle Method for Evaluating the Similarity between Two Chromatographic Fingerprints of Chinese Herb. *Acta pharmaceutica Sinica* 37 (9), 41–45. doi:10.1016/S1350-4177(01)00125-0

Wang, Y., Liu, X.-J., Chen, J.-B., Cao, J. P., Li, X., and Sun, C. D. (2021). Citrus Flavonoids and Their Antioxidant Evaluation. *Crit. Rev. Food Sci. Nutr.* 61(2), 1–22. doi:10.1080/10408398.2020.1870035

Weidinger, S., Beck, L. A., and Bieber, T. (2018). Atopic Dermatitis. *Nat. Rev. Dis. Primers* 4 (1), 1. doi:10.1038/s41572-018-0004-910.1038/s41572-018-0001-z

Xda, B., Sw, A., Wb, C., Wickström, S. A., Wagle, P., Brodesser, S., et al. (2020). Epidermal Mammalian Target of Rapamycin Complex 2 Controls Lipid

Synthesis and Filaggrin Processing in Epidermal Barrier Formation. *J. Allergy Clin. Immunol.* 145 (1), 283–300. e288. doi:10.1016/j.jaci.2019.07.033

Xiong, X., Huang, C., Wang, F., Dong, J., Zhang, D., Jiang, J., et al. (2020). Qingxue Jiedu Formulation Ameliorated DNFB-Induced Atopic Dermatitis by Inhibiting STAT3/MAPK/NF-κB Signaling Pathways. *J. Ethnopharmacology* 270 (4), 113773. doi:10.1016/j.jep.2020.113773

Xu, H. Q., and Hao, H. P. (2004). Effects of Iridoid Total Glycoside from Cornus Officinalis on Prevention of Glomerular Overexpression of Transforming Growth Factor Beta 1 and Matrixes in an Experimental Diabetes Model. *Biol. Pharm. Bull.* 27 (7), 1014–1018. doi:10.1007/s00240-002-0268-z10.1248/bpb.27.1014

Yan, S., Zhao, J., Nagle, D., and Yudong, Z. (2018). "Strategy for Modern Research of Traditional Chinese Medicine Formulae,". *In: Systems Biology and its Application in TCM Formulas Research*, New York: Academic Press, 3–18. doi:10.1016/B978-0-12-812744-5.00001-1

Yang, F., Tanaka, M., Wataya-Kaneda, M., Yang, L., Nakamura, A., Matsumoto, S., et al. (2014). Topical Application of Rapamycin Ointment Ameliorates Dermatophagoides farina Body Extract-induced Atopic Dermatitis in NC/Nga Mice. *Exp. Dermatol.* 23. doi:10.1111/exd.12463

Yang, Y., Zhao, X. J., Pan, Y., and Zhou, Z.(2015). Identification of the Chemical Compositions of Ponkan Peel by Ultra Performance Liquid Chromatography Coupled with Quadrupole Time-Of-Flight Mass Spectrometry. *Anal. Methods* 8 (1), 4. doi:10.1039/C5AY02633D

Yang, Y., Zhi, H., Yan, B., Tian, Y., Shen, J., Zhu, X., et al. (2020). Comparison Study on the Contents of Eight Flavonoids in Three Different Processed Products of Scutellariae Radix Using Ultra-high Performance Liquid Chromatography Coupled with Triple-Quadrupole Mass Spectrometry. *Curr. Pharm. Anal.* 16 (6), 690–697. doi:10.2174/1573412915666190206124150

Yao, Z., Zhang, L., and Ji, G. (2014). Efficacy of Polyphenolic Ingredients of Chinese Herbs in Treating Dyslipidemia of Metabolic Syndromes. *J. Integr. Med.* 12 (003), 135–146. doi:10.1016/S2095-4964(14)60023-6

Yu, M., Zhou, C., Tian, D., Jia, H. M., Li, Z. Q., Yang, C., et al. (2021). Molecular Classification and Clinical Diagnosis of Acute-On-Chronic Liver Failure Patients by Serum Metabolomics. *J. Pharm. Biomed. Anal.* 198 (22), 114004. doi:10.1016/j.jpba.2021.114004

Yuansheng, X., Qing, X., and Yu, J. (2006). Systematic Separation and Preparation of Standard Multi-Component Collectives from Traditional Chinese Medicine. *World Sci. Technology/Modernization TCM Materia Med.* 8 (03), 79–84. doi:10.3969/j.issn.1674-3849.2006.03.018

Zeng, H. R., Zhao, B., Rui, X., Jia, G. H., Wu, Y., Zhang, D., et al. (2021). A TCM Formula VYAC Ameliorates DNCB-Induced Atopic Dermatitis via Blocking Mast Cell Degranulation and Suppressing NF-Kb Pathway. *J. Ethnopharmacology* 280 (12), 114454. doi:10.1016/j.jep.2021.114454

Zhang, A., Sun, H., Han, Y., and Wang, X. (2017). "UPLC/MS and its Potential in Traditional Chinese Medicine Development-ScienceDirect," *In: Serum Pharmacochemistry of Traditional Chinese Medicine*, New York: Academic Press, 23–35. doi:10.1016/B978-0-12-811147-5.00004-2

Zhenyukh, O., Civantos, E., Ruiz-Ortega, M., Sánchez, M. S., Vázquez, C., Peiró, C., et al. (2017). High Concentration of Branched-Chain Amino Acids Promotes Oxidative Stress, Inflammation and Migration of Human Peripheral Blood Mononuclear Cells via mTORC1 Activation. *Free Radic. Biol. Med. Official J. Oxygen Soc.* 104 (3), 165–177. doi:10.1016/j.freeradbiomed.2017.01.009

Zuo, R., Wang, H., Si, N., Zhao, H., Yang, J., and Bian, B. L. (2014). LC-FT-ICR-MS Analysis of the Prototypes and Metabolites in Rat Plasma after Administration of Huang-Lian-Jie-Du Decoction. *Acta Pharmaceutica Sinica* 49 (2), 237–243. doi:10.16438/j.0513-4870.2014.02.006